Journal of Molecular Catalysis, 86 (1994) 129-177
Elsevier Science B.V., Amsterdam

M215

Preparation, characterization, and application of fine metal particles and metal colloids using hydrotriorganoborates

Helmut Bönnemann*, Werner Brijoux, Rainer Brinkmann, Rainer Fretzen, Thomas Joussen, Rainer Köppler, Barbara Korall, Peter Neiteler and Joachim Richter

Max-Planck-Institut für Kohlenforschung, Postfach 10 13 53, W-4330 Mülheim an der Ruhr (Germany)

(Received November 1, 1992; accepted February 1, 1993)

Abstract

The reduction of transition metal salts and oxides using hydrotriorganoborates in organic media allows the production of X-ray amorphous nanopowders of metals and alloys under mild conditions. For example, the reduction of needle-shaped iron oxides at 80°C in organic solvents leads to acicular iron-magnet pigments suitable for recording magnetic signals. The reduction of $TiCl_4$ with $K[BEt_3H]$ gives an ether-soluble $[Ti(0)\cdot 0.5THF]_x$ which serves as a catalyst for the hydrogenation of titanium or zirconium sponges and related systems and as a powerful activator for heterogeneous hydrogenation catalysts. The use of tetraalkylammonium hydrotriorganoborates as reducing agents leads to colloidal transition metals in organic phases. These colloids may also be obtained using conventional reducing agents after first reacting the metal salts with the stabilizing tetraalkylammonium halide. Colloidal metals prepared in this way serve as sources for heterogeneous metal catalysts.

Key words: hydrotriorganoborates; metal colloids; metal particles

Introduction

Finely divided metals and alloys are of considerable interest in industrial powder technology [1] and in catalysis [2]. Fine metallic powders are usually made by metal evaporation [3], electrochemical processes [4], or the chemical reduction of metal salts, either with naphthalene activated alkali metals [5] or with anthracene activated magnesium [6], [7]. Recently we have reported the use of hydrotriorganoborates for the reduction of transition metal salts in organic solvents under mild conditions giving X-ray amorphous nanopowders of metals in the periodic table groups 6–12 and 14 [8]. By coreduction of metal salts the corresponding binary intermetallics were obtained [8]. The reductive deoxygenation of transition metal oxides and e.g. Fe/Ni ternary spinels using

---

*Corresponding author.

SSDI 0304-5102(93)E0148-A

hydrotriorganoborates yields metal powders or intermetallics respectively. The deoxygenation of non-noble metal oxides, however, requires the presence of additional hydrogen. We have exploited this method to transform needle shaped iron oxides into acicular iron magnet pigments [9]. An extension of our preparative concept led to the formation of colloidal transition metals in organic media. An ether soluble Ti(0), stabilized by complexed THF, was isolated by reducing $TiCl_4$ with $K[BEt_3H]$ in THF [10]. A large variation of colloidal transition metals of the groups 6–11 have become accessible by treatment of suspended metal salts in THF with tetraalkylammonium hydrotriorganoborates [11]. The NR_4^+ salts, which are formed in a high local concentration at the reduction centre, act as efficient ligands and prevent aggregation of the metal. Further studies [12] have revealed, that the stabilizing tetraalkylammonium halide may alternatively be prereacted with the metal salt and subsequently reduced with conventional inorganic or organic reagents giving stable, isolable metal colloids having a narrow particle size distribution.

The object of this paper is to review the preparative potential of hydrotriorganoborates as reducing agents for the production of new nanoscale materials. Further, the application of acicular iron powders for magnetic signal recording, the use of the ether-soluble $[Ti(0)\cdot 0.5THF]_x$ as a catalyst for the hydrogenation of metals and as a doping agent for heterogeneous catalysts and finally the catalytic properties of NR_4^+ stabilized colloidal noble metals as liquid-phase hydrogenation catalysts is discussed.

Results and discussion

Finely divided metal and alloy powders from metal salts

Alkali metal tetrahydroborates $M[BH_4]$ (M=Li, Na) in aqueous solution have widely been exploited for the reductive production of transition metal powders [13]. More recently these materials were shown to be generally X-ray amorphous [14]. However, because all of the four hydrogen atoms in the BH_4^- anion can take part in the reducing process, the resulting metal powders are contaminated with borides. For example, the reduction of $NiCl_2$ with $Na[BH_4]$, Eqn. (1), which was introduced on an industrial scale for the deposition of Ni on various supports, gives a nickel powder containing ca. 5% boron in the form of Ni_3B [15].

$$10NiCl_2 + 8NaBH_4 + 17NaOH + 3H_2O \rightarrow (3Ni_3B + Ni) + 5NaB(OH)_4 + 20NaCl + 17.5H_2\uparrow \quad (1)$$

Alkaline hydrotriorganoborates $M[BR_3H]$ [16] may formally be regarded as adducts of MH to BR_3. Here, in contrast, the organoboron part has no reducing properties, but exclusively functions as a complexing agent to generate very soluble metal hydrides in organic media. This allowed us to develop a process for preparing boride free metal nanopowders by reducing metal salts with alkali or alkaline earth metal hydrides in organic phases [8], [17]. The hydrides are solubilized in organic media using BR_3 or $BR_n(OR')_{3-n}$ (R, R' = alkyl or aryl; $n = 0, 1, 2$) as complexing agents to form hydrotriorganoborates [16] of the general formula $M'H_u \cdot (BR_3)_u$ or $M'H_u \cdot [BR_n(OR')_{3-n}]_u$ (M' = alkali or alkaline earth metal, $u = 1, 2$). In an analogous way organogallium compounds $GaR_n(OR')_{3-n}$ ($n = 0, 1, 2, 3$) may be used as complexing agents to give the corresponding hydrotriorganogallates in organic solvents. Elements of groups 6–12 and 14 of the periodic table can be prepared as pure powders by treating their metal salts with hydrotriorganoborates or -gallates in organic solvents between −20 °C and the boiling temperature of the solvent. With the restriction that the solvent should not react with the hydrides, all types of organic media were found to be suitable for the reduction process, Eqn. (2).

$$uMX_v + vM'(BR_3H)_u \xrightarrow{THF} uM\downarrow + vM'(BR_3X)_u + uv/2H_2\uparrow \qquad (2)$$

M = metal powder; M' = alkali or alkaline earth metal; R = C_1–C_6 (alkyl); X = OH, OR, CN, OCN, SCN.

Since the ate complexes formed by reaction of hydroxides, alkoxides, cyanides, and thiocyanates with the triorganoboron and -gallium complexing agents are very soluble in organic solvents, the pure metal powders can be isolated according to Eqn. (2) ($u = 1, 2$) by simple filtration (Table 1). The triorganoboron complexing agent can be regenerated by treatment with acid. Thus, HCl/THF liberates 98% of the triethylborane from $Na[(BEt_3)OH]$.

The redox potential of sodium hydrotriethylborate in THF (supporting electrolyte: Bu_4NPF_6) was determined electrochemically to be −0.77 V [8]. Depending on the particular metal involved, the reaction between the metal salt and the hydride, Eqn. (2), proceeds either as a reduction or as a metathesis. The results can be rationalized on the basis of the HSAB concept [18]. The metal ions M^+ act as soft acids and compete with the moderately hard acid BR_3 [19] for the soft basic hydride to form **1**. If M^+ is a softer acid than BR_3, the hydride is transferred to M^+, the resulting MH then decomposes spontaneously to give metal and hydrogen, Eqn. (3).

$$MX + M'(BR_3H) \xrightarrow{-M'X} \underset{\mathbf{1}}{(M\cdots H\cdots BR_3)} \longrightarrow [MH] + BR_3 \xrightarrow{-BR_3} M\downarrow + 1/2H_2\uparrow \qquad (3)$$

Metal halides do not generally form stable ate complexes. In many cases, however, after the reduction, Eqn. (4), they remain dissolved in the organic phase along with the liberated BR_3. This was observed particularly when using THF in the case of LiCl, LiBr, LiI, and NaI. To obtain pure metal powders according to Eqn. (4) in one step, the cation in the hydride has to be chosen so that the M' halide dissolves in the solvent. If the M' halide precipitates

TABLE 1

Preparation of nanocrystalline metal powders in THF with formation of soluble borates [Eqn. (2)][a]

No.	Metal salt	Reducing agent	Conditions		Product	
			t (h)	T (°C)	Metal content (%)	Boron content (%)
1	$Fe(OEt)_2$	$NaBEt_3H$	16	65	96.8	0.16
2	$Co(OH)_2$	$NaBEt_3H$	2	23	94.5	0.40
3	$Co(CN)_2$	$NaBEt_3H$	16	65	96.5	0.20
4[a]	$Ni(OH)_2$	$NaBEt_3H$	2	23	94.7	0.13
5	$Ni(OEt)_2$	$NaBEt_3H$	16	65	91.4	0.58
6	CuCN	$LiBEt_3H$	2	23	97.3	0.0
7	CuSCN	$NaBEt_3H$	16	65	95.0	0.23
8	$Pd(CN)_2$	$NaBEt_3H$	16	65	95.5	1.38
9	AgCN	$Ca(BEt_3H)_2$[b]	2	23	89.6	0.20
10	$Cd(OH)_2$	$NaBEt_3H$	2	23	97.9	0.22
11	$Pt(CN)_2$	$NaBEt_3H$	16	65	87.5	0.93
12	AuCN	$NaBEt_3H$	2	23	97.5	0.0

[a] For a typical procedure see Experimental.
[b] Solvent: diglyme.

(e.g., NaCl), it must be separated from the metal powder by washing with water.

$$uMX_v + vM'(BR_3H)_u \xrightarrow{THF} uM\downarrow + vM'X_u + uvBR_3 + uv/2H_2\uparrow \quad (4)$$

X = halogen.

The reduction of metal halides in organic phases can also be achieved by adding only a catalytic amount of BR_3 to suspended $M'H_u$. The organoboron complexing agents liberated according to Eqn. (4) react with further metal hydride in suspension to regenerate the hydrotriorganoborate complexes in situ [Eqn. (5), Table 2, Nos. 6 and 24].

$$uMX_v + vM'H_u \xrightarrow{BR_3,\ THF} uM\downarrow + vM'X_u + uv/2H_2\uparrow \quad (5)$$

X = halogen.

Tetrabutylammonium hydrotriorganoborates, which are readily accessible from ammonium halides and alkali metal hydrotriorganoborates [11] may advantageously be used for the reduction of metal halides in THF. Because the ammonium halides formed as the byproducts according to Eqn. (6) remain completely dissolved after the reaction, the precipitated metal powders can easily be isolated in pure form.

TABLE 2

Preparation of nanocrystalline metal powders in THF [Eqn. (4)][a]

No.	Metal salt	Reducing agent	Conditions		Product	
			t (h)	*T* (°C)	Metal content (%)	Boron content (%)
1	$CrCl_3$	$NaBEt_3H$	2	23	93.3	0.3
2	$MnCl_2$	$LiBEt_3H$	1	23	94.0	0.42
3	$FeCl_3$	$LiBEt_3H$	2	23	97.1	0.36
4	CoF_2	$NaBEt_3H$	16	65	96.9	0.0
5	$CoCl_2$	$NaBEt_3H$	16	65	95.1	0.0
6	$CoCl_2$	LiH + 10% BEt_3	16	65	95.8	0.0
7	$CoBr_2$	$LiBEt_3H$	2	23	86.6	0.0
8	$NiCl_2$	$NaBEt_3H$	16	65	96.9	0.0
9	$CuBr_2$	$LiBEt_3H$	2	23	94.9	0.0
10	$CuCl_2$	$Na(Et_2BOMe)H$	2	23	94.7	0.1
11	$ZnCl_2$	$LiBEt_3H$	12	65	97.8	0.0
12	$RuCl_3$	$NaBEt_3H$	16	65	95.2	0.52
13	$RhCl_3 \times 3H_2O$	$NaBEt_3H$	2	23	98.1	0.1
14	$RhCl_3$	$LiBEt_3H$	2	23	96.1	0.66
15	$PdCl_2$	$NaBEt_3H$	16	65	98.0	0.29
16	AgF	$NaB(OMe)_3H$	2	23	94.1	0.05
17	AgJ	$NaBEt_3H$	2	23	95.3	0.02
18	$CdCl_2$	$LiBEt_3H$	2	23	99.4	0.0
19	$ReCl_3$	$LiBEt_3H$	2	23	95.4	0.0
20	$OsCl_3$	$NaBEt_3H$	2	23	95.8	0.0
21	$IrCl_3 \times 4H_2O$	$NaBEt_3H$	216	23	77.1	0.16
22	$IrCl_3$	$KBPr_3H$	2	65	94.7	0.08
23	$PtCl_2$	$NaBEt_3H$	5	23	98.2	0.21
24	$PtCl_2$	LiH + 10% BEt_3	12	65	98.8	0.0
25[a]	$PtCl_2$	$LiBEt_3H$	4	65	99.0	0.0
26	$PtCl_2$	$LiBEt_3H$	2	0	99.0	0.0
27	$SnCl_2$	$LiBEt_3H$	2	23	96.7	0.0
28	$SnBr_2$	$LiBEt_3H$	2	23	87.1	0.0
29[a]	$PdCl_2$	$Na(GaEt_2OEt)H$	2	40	92.7	Ga: 0.25
30	$Pt(NH_3)_2Cl_2$	$NaBEt_3H$	2	23	97.1	0.32
31	$Pt(Py)_2Cl_2$	$LiBEt_3H$	2	23	97.1	0.02
32	$Pt(Py)_4Cl_2$	$LiBEt_3H$	2	23	97.5	0.01
33	$CODPtCl_2$	$NaBEt_3H$	2	60	97.9	0.58

[a] For a typical procedure see Experimental.
Py = pyridine.
COD = 1,5-cyclooctadiene.

$$MX_v + vNR_4(BEt_3H) \xrightarrow{THF} M\downarrow + vNR_4X + vBEt_3 + v/2H_2\uparrow \qquad (6)$$

X = halogen; $v = 1, 2, 3$; R = *n*-butyl.

Some typical examples of variant, Eqn. (6), for the preparation of nanopowders from metal halides are summarized in Table 3.

The metal powders were characterized by electron microscopy, X-ray dif-

TABLE 3

Preparation of nanocrystalline metal powders in THF [Eqn. (6)][a]

No.	Metal salt	Reducing agent	Conditions		Product	
			t (h)	*T* (°C)	Metal content (%)	Boron content (%)
1	$CoCl_2$	NBu_4BEt_3H	3	23	93.6	0.3
2	$PdCl_2$	NBu_4BEt_3H	3	23	96.2	0.47
3	$PtCl_2$	NBu_4BEt_3H	3	23	97.8	0.2
4	AgCl	NBu_4BEt_3H	3	23	98.0	0.2
5	$AuCl_3$	NBu_4BEt_3H	3	23	97.5	0.2
6	$CODPdCl_2$	NBu_4BEt_3H	3	23	86.7	0.2

[a] For a typical procedure (analogous to TABLE 2 No.25) see Experimental.
COD = 1,5-cyclooctadiene.

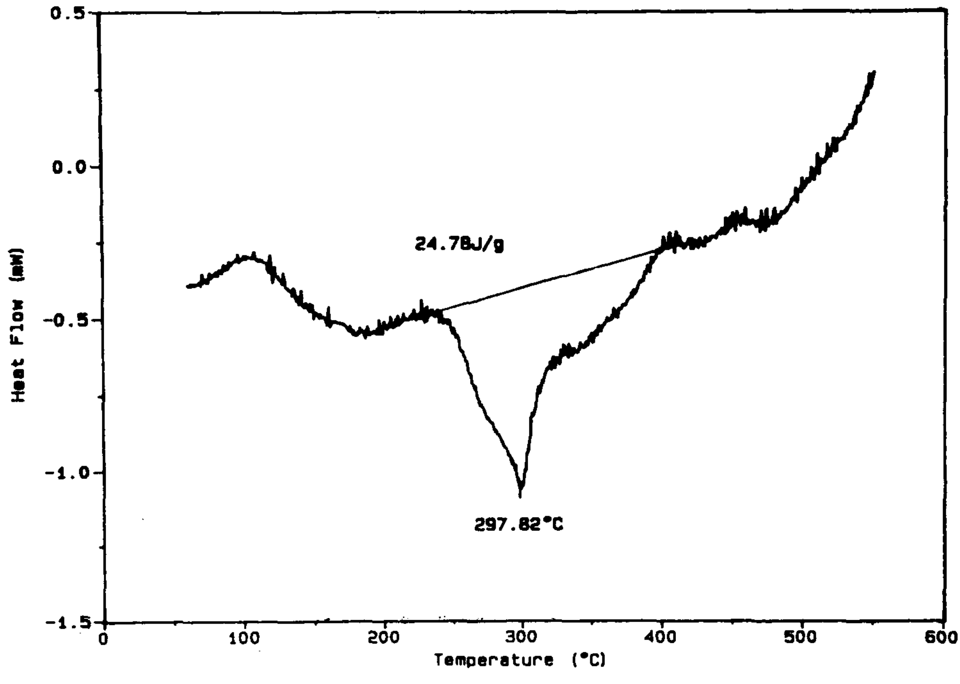

Fig. 1. DSC diagram of nanocrystalline cobalt powder (Table 2, No. 5). Heating rate: 5 K/min.

fractograms, and differential scanning calorimetry studies. The DSC diagram (Fig. 1) of a boron free cobalt sample, obtained from $CoCl_2$ according to Eqn. (4) (Table 2, No. 5), shows endothermic recrystallization of the powder between 230°C and 400°C. A second run made sure that the thermal recrystallization was complete.

At 298°C a heat flow minimum is seen. For the recrystallization of the sample an enthalpy difference of ΔH_R(Co) = 24.78 J/g was calculated. A comparison of the melt and recrystallization enthalpy values allows to draw conclusions about the crystallinity of a given sample. The melt enthalpy value ΔH_F (Co) is 259.63 J/g [20]. Since the value of ΔH_R(Co) was found to be only ca. 9.5% of the melt enthalpy ΔH_F(Co) quoted, it was concluded, that the cobalt powder measured was nanocrystalline.

An inspection of the line widths in the X-ray diffractograms has revealed that the obtained metal powders (Tables 1–3) are generally nanocrystalline (X-ray amorphous). For example, in Fig. 2 the X-ray diffractogram of a cobalt powder (Table 2, No. 5) before (a) and after (b) annealing at 450°C is shown.

The original sample (a) shows a very diffuse line which is typical for nanocrystalline to X-ray amorphous phases [21]. After annealing four sharp lines (b) are recorded, the strongest at a scattering angle 2θ of 51.9° and a reciprocal lattice distance d of 2.04 Å. Since the mean particle size of the cobalt powder (100 nm) was found by SEM (scanning electron microscopy) to be identical before and after the annealing the sharp line (b) in Fig. 2 has to be assigned to a thermal augmentation of the grains (nanocrystallites) inside the cobalt particles.

Table 4 summarizes the grain sizes of selected metal powders prepared by the hydrotriorganoborate reduction method, observed by TEM (transmission electron microscopy).

The particle and grain size of the different materials and the statistical size distributions obviously depend rather strongly on the different elements.

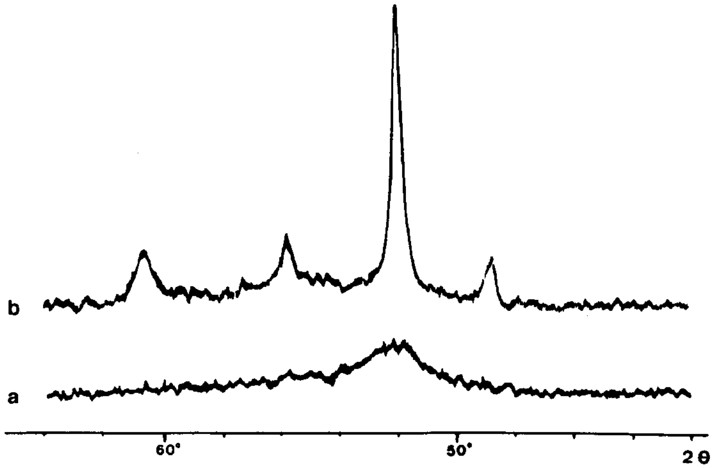

Fig. 2. X-ray diffractogram of cobalt powder (CoK_α-irradiation, Fe filter). (a) Untreated original sample after reduction (nanocrystalline to X-ray amorphous). (b) After 3 h at 450°C, Co (hcp and/or fcc).

TABLE 4

Selected grain sizes of metal powders measured by TEM

No.	Metal	Starting materials	Preparation	Grain size (nm)
1	platinum	$PtCl_2$ $LiBEt_3H$	Table 2, No. 25	2-5
2	palladium	$PdCl_2$ $LiBEt_3H$	similar to Table 2, No. 15	12-28
3	rhodium	$RhCl_3$ $LiBEt_3H$	Table 2, No. 14	1-4
4	copper	$CuCl_2$ $LiBEt_3H$	similar to Table 2, No. 9	25-90
5	nickel	$Ni(OH)_2$ $NaBEt_3H$	Table 1, No. 4	5-15
6	cobalt	$CoCl_2$ $NaBEt_3H$	Table 2, No. 5	3-5

However, metal powders having a very uniform size distribution may be obtained from colloidal metal solutions (vide infra).

In 1986 Van Wontherghem et al. reported the formation of nanoscale X-ray amorphous alloy particles by coreduction of $FeSO_4$ and $CoCl_2$ (molar ratio 7:3) by an excess of $K[BH_4]$ in aqueous solution, Eqn. (7) [22]. From chemical analysis of the particles the formula $Fe_{44}Co_{19}B_{37}$ was derived, and further the low saturation magnetization values of the sample before (89 J T^{-1} kg^{-1}) and after annealing (166 J T^{-1} kg^{-1}) indicated the presence of boron in the alloy or in a separate phase. Since all four hydrogen atoms in BH_4^- take part in the reduction process, Eqn. (7), 7.85% boron is incorporated in the $Fe_{30}Co_{70}$ alloy which was originally targeted.

$$\underset{7}{FeSO_4} + \underset{3}{CoCl_2} \xrightarrow[H_2O/RT]{KBH_4} Fe_{44}Co_{19}B_{37} \qquad (7)$$

$$7 : 3$$

However, using hydrotriorganoborates, the simple coreduction of a mixture of different metal salts – dissolved or plainly suspended in THF – according to Eqns. (2) and (4) affords practically boron free nanocrystalline alloys of two and more metals (Table 5). Within the limits of miscibility of the particular metals, known from the phase diagrams, the atomic ratio of the metals in the alloys may be adjusted by altering the proportion of the starting materials. For example, the coreduction of $FeCl_3$ and $CoCl_2$ in the molar ratio of 7:3 according to Eqn. (4) yields a boron free $Fe_{70}Co_{30}$ powder (Table 5, No. 3). In the diffractogram only the diffuse strongest reflection at a scattering angle 2θ of 52.5° and a reciprocal lattice distance d of 2.02 Å can be discerned (Fig. 3a). The line width reveals that weakly crystalline to amorphous phases are present in the Fe/Co powder. After annealing (2 h, 400°C) the line becomes sharper (Fig. 3b). Since electron microscopy shows the particle size to be unchanged after annealing, the sharpening of the peak indicates that the grain size within the particles was increased by the heat treatment.

A comparison of the diffractograms of the alloy with that of a mixture of amorphous iron and cobalt powders (Fig. 4a) demonstrates, that the $Fe_{70}Co_{30}$

TABLE 5

Preparation of nanocrystalline alloys by coreduction of metal salts in THF [a]

No.	Metal salt	Reducing agent	Conditions		Product		DIF[b]		Comments
			t (h)	T (°C)	Metal content (%)	Boron content (%)	2θ[c] (°)	D[d] (Å)	
1	$Co(OH)_2$	$NaBEt_3H$	7	65	Co: 48.3	0.25	51.7	2.05	single phase
	$Ni(OH)_2$				Ni: 45.9				nanocrystalline
2	$FeCl_3$	LiH + 10% BEt_3	6	65	Fe: 47.0	0.0	52.7	2.02	single phase
	$CoCl_2$				Co: 47.1				grain size: 1-5 nm
3[a]	$FeCl_3$	$LiBEt_3H$	5	23	Fe: 54.8	0.0	52.5	2.02	single phase
	$CoCl_2$				Co: 24.5		99.9	1.17	nanocrystalline
4	$CoCl_2$	$LiBEt_3H$	7	65	Co: 21.6	0.0	55.4	1.93	single phase
	$PtCl_2$				Pt: 76.3		47.4	2.23	
5	$RhCl_3$	$LiBEt_3H$	5	65	Rh: 26.5	0.04	40.2	2.24	single phase
	$PtCl_2$				Pt: 65.5		46.3	1.96	grain size: 1-4 nm[e]
6	$RhCl_3$	$LiBEt_3H$	5	65	Rh: 33.5	0.15	42.3	2.14	single phase +
	$IrCl_3$				Ir: 62.5				traces $IrCl_3$
7	$PdCl_2$	$LiBEt_3H$	5	65	Pd: 33.6	0.04	40.1	2.25	single phase
	$PtCl_2$				Pt: 63.4		46.3	1.96	grain size: 2-6 nm[e]
8[a]	$PtCl_2$	$NaBEt_3H$	12	65	Pt: 50.2	0.15	40.0	2.25	single phase
	$IrCl_2$				Ir: 48.7		46.5	1.95	nanocrystalline
9	$CuCl_2$	$LiBEt_3H$	4	65	Cu: 49.6	0.0	30.2	2.96	Cu_6Sn_5 +
	$SnCl_2$				Sn: 47.6		53.5	1.80	Cu + Sn
10	$FeCl_3$	$LiBEt_3H$	1.5	23	Fe: 30.1	0.0	52.7	2.02	single phases
	$CoCl_2$				Co: 31.4		60.8	1.77	nanocrystalline
	$NiCl_2$				Ni: 30.9		77.7	1.43	
							100.3	1.17	

[a] For a typical procedure see Experimental.
[b] X-ray diffractogram, CoK_α irradiation, Fe-filter.
[c] Strongest reflections.
[d] Reciprocal lattice distance.
[e] Measured by TEM

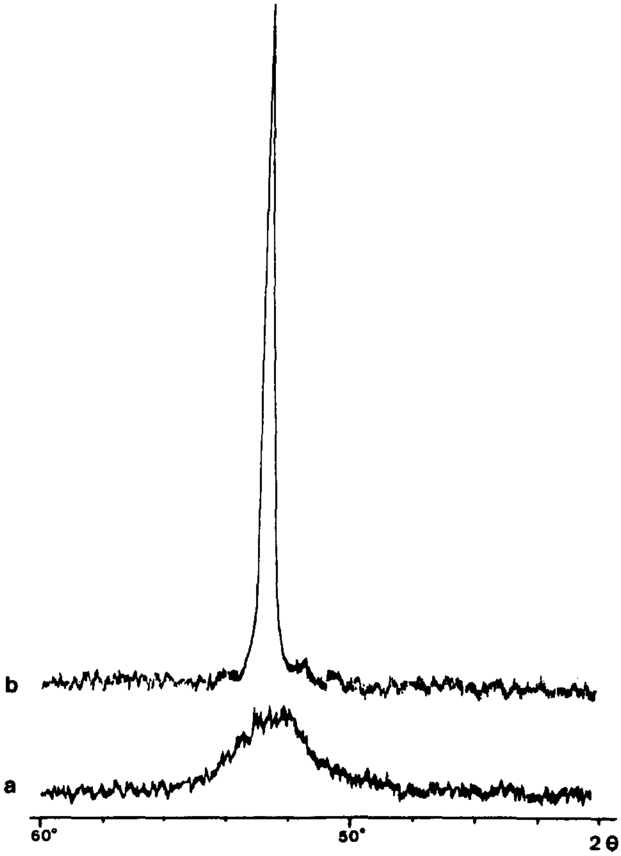

Fig. 3. Strongest reflection in the diffractogram of an Fe/Co alloy (Table 5, No. 3). (a) Untreated original sample. (b) After 2 h at 400°C (CoK$_\alpha$-irradiation with Fe filter).

alloy is formed at the stage of the coreduction under thermodynamic control and not as a result of the subsequent heat treatment: after annealing the diffractogram of the Fe/Co mixture (Fig. 4b) is, in contrast to that of the alloy, a superimposition of the two sets of lines for Fe and Co.

An unambiguous proof that a Fe/Co alloy had been formed as a result of the coreduction was provided by the comparison of a Mössbauer spectrum (source: ^{57}Co/Pt, 27°C) of a $Fe_{64}Co_{36}$ sample prepared by coreduction with the known spectrum of a sample of the same composition [23] provided by melt metallurgy (Fig. 5).

In the Mössbauer spectrum of $Fe_{64}Co_{36}$ produced by coreduction of $FeCl_3$ and $CoCl_2$ (Fig. 5a) the six resonances for metallic iron can be identified. The overall splitting (i.e. the distance between the outer lines) is 36 T. The $Fe_{60}Co_{40}$ sample made by melt metallurgy for comparison gives an identical spectrum (Fig. 5b) which confirms that iron and cobalt are in fact completely alloyed in the sample prepared by the coreduction.

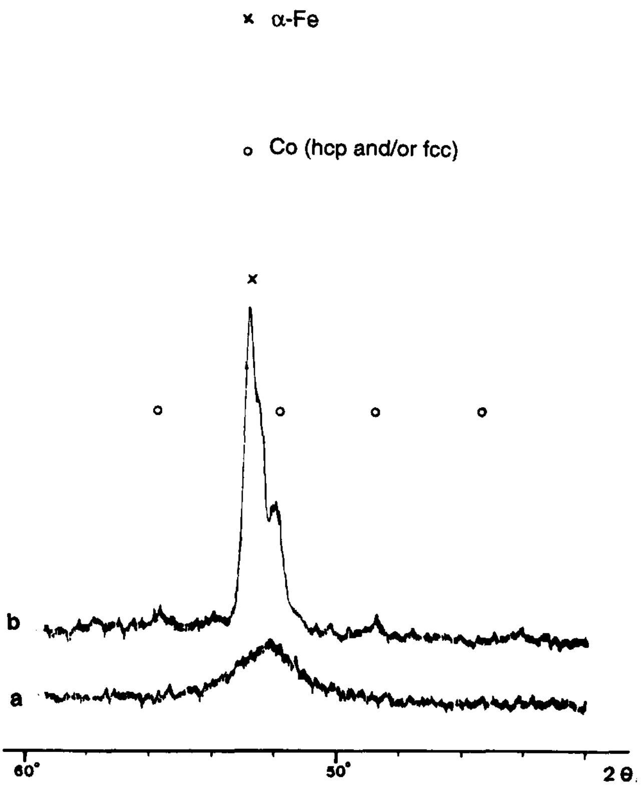

Fig. 4. Strongest reflection in the diffractogram of an Fe/Co mixture. (a) Untreated original sample. (b) After 2 h at 400°C (CoK_α irradiation, Fe filter).

The coreduction of metal salts with hydrotriorganoborates in organic solvents provides a general route for the preparation of single phase, X-ray amorphous alloys of two or more components (Table 5). Recently Hampden-Smith extended this method for the room temperature synthesis of Mo_2C and W_2C through the reduction of THF suspensions of $MoCl_4 \cdot 2THF$, $MoCl_3 \cdot 3THF$, and WCl_4 with $Li[BEt_3H]$ [24].

Metal and alloy powders from metal oxides

In analogy to Eqn. (2) hydrotriorganoborates in organic phases can also be used for the reduction of transition metal oxides to give practically boron free metal powders under mild conditions. The deoxygenation of HgO, PtO_2, Ag_2O, and PdO in various organic media takes place very smoothly even at moderate temperatures (Table 6, Nos. 1–5). The course of the reaction has not been elucidated yet in every detail; presumably the first step of the deoxygention consists in the transformation of the metal oxo group to the corresponding metal hydroxide, which is due to subsequent reduction. This assumption is supported by the fact, that the application of an excess of the hydrotriorga-

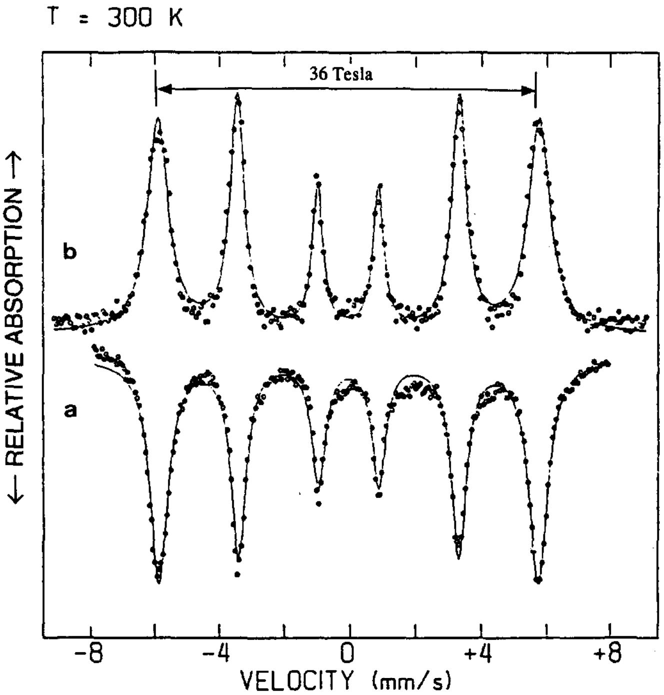

Fig. 5. Mössbauer spectrum of (a) $Fe_{64}Co_{36}$ alloy obtained by coreduction, (b) $Fe_{60}Co_{40}$ alloy obtained by melting. Source: $^{57}Co/Pt$, 27 °C.

noborates is advantageous in order to afford a clean and complete deoxygenation of the metal oxides. Because the hydroxotriorganoborates formed as the byproducts readily dissolve in organic solvents, the metal powders can be isolated by simple filtration. The overall reaction is represented by Eqn. (8), which describes the deoxygenation of PtO_2 (Table 6, No. 2).

$$PtO_2 + NaBEt_3H\ (\text{excess}) \xrightarrow{\text{4h, 20°C, THF}} Pt\downarrow + NaBEt_3OH \qquad (8)$$

The reduction of less noble metal oxides, such as CuO, may be improved by additional hydrogen in the reaction mixture as can be deducted from the purity of the resulting copper powders (Table 6, Nos. 6 and 7) by comparison. In contrast, the deoxygenation of typical non-noble metal oxides by hydrotriorganoborates requires the presence of compressed hydrogen (Table 6, Nos. 8–15).

X-ray powder diffraction measurements have revealed that the metal powders obtained by the deoxygenation of metal oxides are generally nanocrystalline. The grain size of the nickel and cobalt powders quoted in Table 6 was determined by TEM to range between 6–10 nm (Nos. 8 and 9) and 1–5 nm (Nos. 10–12).

An interesting application of the deoxygenation reaction described above

TABLE 6

Preparation of nanocrystalline metal powders from metal oxids in org. solvents [a]

No.	Metal oxide	Reducing agent	Solvent	Conditions			Product	
				H_2 pressure (bar)	*t* (h)	*T* (°C)	Metal content (%)	Boron content (%)
1	HgO	$NaBEt_3H$	toluene	-	16	20→90	97.72	1.21
2[a]	PtO_2	$NaBEt_3H$	THF	-	4	20	97.54	0.55
3	Ag_2O	$NaBEt_3H$	toluene	-	16	20	97.66	0.10
4	Ag_2O	$NaBEt_3H$	triglyme	-	16	20	97.95	0.13
5	PdO	$NaBEt_3H$	toluene	-	16	80	98.22	0.03
6	CuO	$NaBEt_3H$	toluene	-	16	20	89.8	0.0
7	CuO	$NaBEt_3H$	toluene	100	16	130	96.3	0.0
8	NiO	$NaBEt_3H$	toluene	100	16	130	94.05	0.0
9	NiO	$NaBEt_3H$	THF	100	16	130	98.4	0.13
10	CoO	$NaBEt_3H$	toluene	3	16	130	98.1	-
11	CoO	$NaBEt_3H$	toluene	100	4	130	97.96	-
12	CoO	$KBEt_3H$	THF	100	16	130	97.2	0.28
13[a]	FeOOH	$NaBEt_3H$	toluene	100	16	80	87.87	-
14	FeOOH	$NaBEt_3H$	THF	100	16	80	87.5	-
15	Fe_2O_3	$NaBEt_3H$	toluene	100	16	80	88.3	-

[a] For a typical procedure see Experimental;

consists in a process for the transformation of finely divided, needle-shaped iron oxides into acicular iron magnet pigments for magnetic signal recording [25]. The conventional industrial process for the production of acicular iron pigments from the corresponding iron oxides or oxide-hydroxides by reduction with excess gaseous hydrogen, Eqn. (9), generally affords temperatures above 250°C in the fluid bed reactor [26].

$$\alpha\text{-}Fe_2O_3 + 3H_2 \overset{400^\circ C,\ 16\ h}{\rightleftharpoons} 2Fe_{acicular} + 3H_2O \qquad (9)$$

However, the process, Eqn. (9), is associated with the inherent disadvantage that the very labile acicular iron pigments break or agglomerate at the high temperatures used in the fluid bed reactor because of unwanted sintering effects. Using hydrotriorganoborates in the presence of compressed hydrogen (20–100 bar), we were able for the first time to reduce iron oxides to yield well shaped acicular iron particles at only 80°C (Eqn. 10 and 11).

$$\alpha\text{-}FeOOH + 2NaBEt_3H \xrightarrow{20\ bar\ H_2,\ 80^\circ C,\ 4\ h} Fe_{acicular} + 2NaBEt_3OH \qquad (10)$$

$$\alpha\text{-}Fe_2O_3 + 3NaBEt_3H \xrightarrow{20\ bar\ H_2,\ 80^\circ C,\ 4\ h} 2Fe_{acicular} + 3NaBEt_3OH \qquad (11)$$

The metal oxide is suspended in organic solvents and treated with the combination of molecular hydrogen and the soluble hydrotriorganoborates. Surprisingly, under these mild reaction conditions the oxygen may be removed from the iron oxide lattice quantitatively. The pyrophoric iron pigments may be isolated from the clear organic solution by filtration. The trialkylborane acts as a complex carrier in organic solution both for the metal hydride and the resulting metal hydroxide and may be reused after hydrolysis of the triorganohydroxoborate. The regeneration amount of the carrier exceeds 97% [25] (See Experimental). Fig. 6 shows a TEM image of the α-FeOOH used as the starting material for the deoxygenation reaction, Eqn. (10), (Table 6, No. 13). Well shaped small needles of ca. 350 nm length appear at a magnification of 50 000 : 1. Although, relative to the starting material, upon the reaction forming the metal pigment a volume decrease by about 60% is observed, the needle shape of the α-FeOOH is retained according to the TEM findings. The product shown in Fig. 7 at the same scale consists of an acicular iron pigment of ca. 250 nm length and a diameter of ca. 20 nm, and does not exhibit any sintering.

The acicular iron pigments prepared according to Eqns. (10) and (11) were found to have superior magnetic properties. The crucial characteristics

Fig. 6. TEM image of α-FeOOH (Table 6, No. 13).

Fig. 7. TEM image of Fe (Table 6, No. 13).

of magnetic materials for recording purposes are saturation magnetization M_S, remanence M_R, and coercive field strength H_C. In practice an adjustment of certain coercive force ranges H_C of the magnet pigment to be used is desirable. Whereas the magnetic properties of iron pigments from the high temperature gas phase reduction process, Eqn. (9), can be varied only via the particle size and shape of the iron oxide starting compounds, the low temperature deoxygenation according to Eqns. (10) and (11) allows to prepare acicular iron pigments which exhibit high values of the saturation magnetization M_S and remanence M_R along with a coercive force value which can be adjusted for the special sector of application simply by thermal after-treatment without causing undesirable sintering of the metal needles. An inspection of Table 7 shows, that the H_C-value of the iron pigment quoted in Table 6, No. 13 may be increased from 82 kA/m in the initial product to >100 kA/m by thermal treatment at $>200\,^\circ$C in hydrogen or argon atmosphere or in vacuo. Probably this is a consequence of an augmentation of the grains (nanocrystals) present in the acicular particles during the annealing.

Using the combination of hydrotriorganoborates and compressed hydro-

TABLE 7

Adjustment of the coercive field force H_C of Fe powder (Table 6, No. 13) by thermal after-treatment (4h)

After-treatment	M_S (mT cm^3/g)	M_R (mT cm^3/g)	H_C (kA/m)
without	193.0	101.3	82.2
150°C (H_2-atmosphere)	-	-	83.0
200°C (H_2-atmosphere)	-	-	99.8
250°C (H_2-atmosphere)	199.0	111.6	101.6
250°C (Ar-atmosphere)	204.0	114.0	100.4
250°C (vacuum)	203.0	113.0	101.4
300°C (H_2-atmosphere)	-	-	98.2

gen, the deoxygenation of mixed oxides can be achieved under mild conditions giving nanocrystalline alloy powders (Table 8). For example, the ternary spinel $NiFe_2O_4$ can be transferred smoothly into a single phase $NiFe_2$ at 130°C in toluene (Eqn. 12, Table 8, No. 2).

$$NiFe_2O_4 + 4NaBEt_3H \xrightarrow[\text{toluene}]{\text{100 bar } H_2\text{, 130°C}} NiFe_2 + 4NaBEt_3OH \qquad (12)$$

Surprisingly, the preparation of nanocrystalline metal alloys can also be achieved by the deoxygenation of metal oxide mixtures suspended in organic media, under analogous reaction conditions to those of Eqn. (12). The advantage of this variation is that the ratio of the metals in the resulting alloys can be adjusted by varying the ratio of the metal oxides in the starting materials. X-ray diffractometry has confirmed the presence of metal alloys in the products and excluded the contamination by non-alloyed metals in their elemental form (See Table 8).

Formation of colloidal transition metals and alloys in organic solvents

Because of their potential in catalysis, colloidal mono- and bimetallic materials have, after a period of hibernation, recently attracted more attention, notably through the contributions of Bradley [27], Esumi [28], Klabunde [29], Lewis [30], Moiseev [31], Schmid [32], and Toshima [33]. In the course of our investigations we have developed a new method for the preparation of stable and very soluble metal colloids in organic phases having a narrow particle size distribution. The metal cores derived from elements of the periodic table groups 6–11 are protected by tetraalkylammonium halides [11]. However, in the case of Ti(0), the metal stabilization was achieved by the solvent THF and an ether soluble compound $[Ti(0) \cdot 0.5THF]_x$ has been isolated [10]. Various colloids of this new type have been used to prepare active liquid phase hydrogenation catalysts [34].

TABLE 8

Preparation of alloys from spinels and metal oxides in org. solvents[a]

No.	Metal oxide	Reducing agent	Solvent	Conditions			Product		DIF[b]		Comments
				H_2 pressure (bar)	*t* (h)	*T* (°C)	Metal content (%)	Boron content (%)	2θ[c] (Å)	*D*[d]	
1	$CoNiO_2$	$NaBEt_3H$	toluene	100	16	130	Co: 45.3 Ni: 45.9	0.0	52.1	2.04	single phase (fcc)
2[a]	$NiFe_2O_4$	$NaBEt_3H$	toluene	100	16	130	Ni: 29.0 Fe: 63.67	0.0	52.3	2.03	single phase (bcc)
3	$CoFe_2O_4$	$NaBEt_3H$	THF	100	16	120	Co: 30.3 Fe: 61.1	0.45	52.5	2.02	single phase (bcc)
4	CoO NiO	$NaBEt_3H$	toluene	100	16	130	Co: 43.7 Ni: 47.9	0.48	52.1	2.04	single phase (fcc)
5	NiO Fe_2O_3	$NaBEt_3H$	toluene	100	16	130	Ni: 48.5 Fe: 47.2	0.27	52.2	2.03	single phase (fcc)
6	CoO Fe_2O_3	$NaBEt_3H$	toluene	100	16	130	Co: 48.7 Fe: 48.4	0.36	52.2	2.03	single phase (fcc)

[a] For a typical procedure see Experimental.

[b] X-ray diffractogram, CoK_α irradiation, Fe-filter.

[c] Strongest reflection.

[d] Reciprocal lattice distance.

Ether soluble Ti(0) [10]

The reduction of $TiCl_4\cdot 2THF$ or $TiCl_3\cdot 3THF$ in THF solution with $K[BEt_3H]$ within 2 h gives a brown–black solution under the evolution of H_2 from which about 90% of the precipitated KCl can be removed by filtration. After vacuum evaporation of the solvent and BEt_3 (identified by ^{11}B-NMR spectroscopy) a black residue is obtained which is extracted with THF. This THF solution is treated with pentane to give a brown–black precipitate **2** (Eqn. 13). After thorough drying in vacuo the pyrophoric powder **3** is obtained along with small amounts of KCl (identified by X-ray diffraction). Quantitative measurements of the gas evolved during the reduction (1 mol H_2 per mol Ti), protonolysis of **2** and cross experiments using $K[BEt_3D]$ as the reducing agent in Eqn. (13) show that **2** still has various amounts of residual hydrogen. The hydrogen in **2** is removed in vacuo to give **3**, Eqn. (13). **3** readily dissolves in THF and ether but is insoluble in hydrocarbons such as pentane. For experimental details see [10].

$$x\ [TiCl_4\cdot 2THF] + x\ 4K[BEt_3H] \xrightarrow[2\ h,\ 40^\circ C]{THF}$$

$$\underset{\mathbf{2}}{[TiH_m\cdot 0.5THF]_x} + x\ 4BEt_3 + x\ 4KCl + x\ (2-m/2)H_2\uparrow$$

$$\text{vacuum}\ \Bigg\downarrow \begin{array}{l} -BEt_3 \\ -THF \\ -H_2 \end{array}$$

$$\underset{\mathbf{3}}{[Ti\cdot 0.5THF]_x} \qquad (13)$$

The IR spectrum of **2** shows intact THF coordinated to the metal core. Further characterization of **2** by X-ray diffractometry, XPS, and EXAFS [10] supports its description as colloidal titanium stabilized by complexed THF and containing residual hydrogen (Fig. 8).

The determination of the particle size of this extremely oxophilic titanium colloid by TEM is in progress.

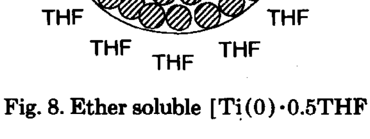

Fig. 8. Ether soluble $[Ti(0)\cdot 0.5THF]_x$.

Besides the application of **2** or **3** as dopant for noble metal hydrogenation catalysts (vide infra), the colloidal $[Ti(0)\cdot 0.5THF]_x$ has been found to be a very efficient catalyst for the hydrogenation of titanium and zirconium sponges as well as for a nickel hydride battery alloy. The uncatalyzed hydrogenation of titanium or zirconium sponges using compressed hydrogen affords pressures above 100 bar and minimum reaction temperatures of 150°C. The hydrogenation of these metals under such drastic conditions, however, is associated with unwanted sintering of the materials so that the products can only be used after additional grinding. After the addition of 1% Ti (present in **3**) to the metal sponges a smooth hydrogenation of titanium and zirconium is observed at low temperatures (60°–90°C). The reaction may be carried out in THF solution, toluene suspension or in the dry state after depositing the catalyst on the surface of the samples by evaporation of the solvent in vacuo. Using a special device [35], the mass specific uptake of hydrogen depending on pressure, temperature and time was monitored automatically. Fig. 9 shows the typical course of the hydrogen uptake during the hydrogenation of a titanium sponge at 60°C catalyzed by 1% Ti in the form of **3**. After a certain latent period with only negligible uptake of H_2 an abrupt start of the catalytic hydrogenation occurs; followed by a period of rather constant H_2 uptake (denoted as the hydrogenation period). Towards the end of the H_2 uptake the reaction turns into a slow decay.

An inspection of Fig. 10 shows, that the mass specific hydrogenation time [min/g] detected for 1 g of titanium sponge at 100 bar H_2 in the presence of the catalyst is constant between 60° and 90°C, practically constant in THF and toluene and even in the absence of a solvent. Significant differences, however, occur with regard to the latent period. If the catalytic hydrogenation of titanium sponge is performed at very low hydrogen pressure (5 bar), a pro-

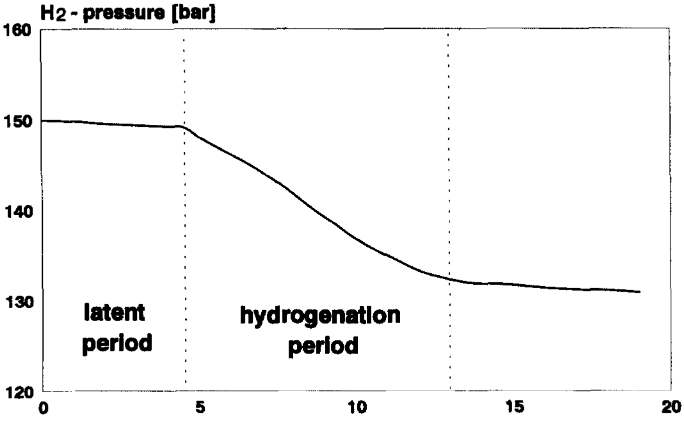

Fig. 9. Hydrogenation of Ti sponge catalyzed by **3**.

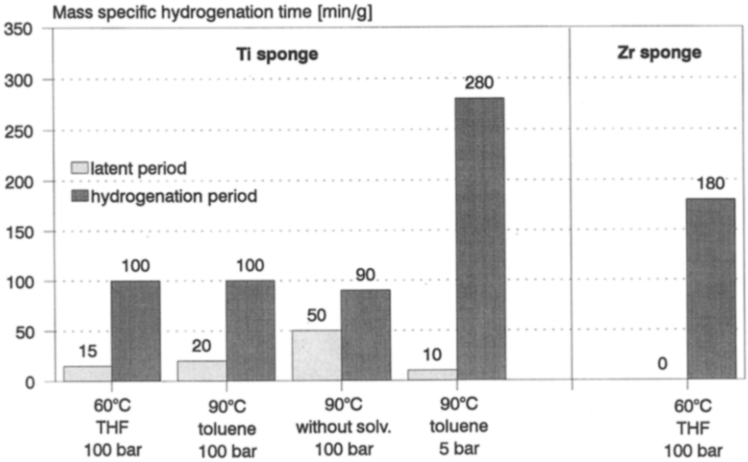

Fig. 10. Influence of temperature, solvent, and pressure in the hydrogenation of Ti and Zr sponges catalyzed by **3**.

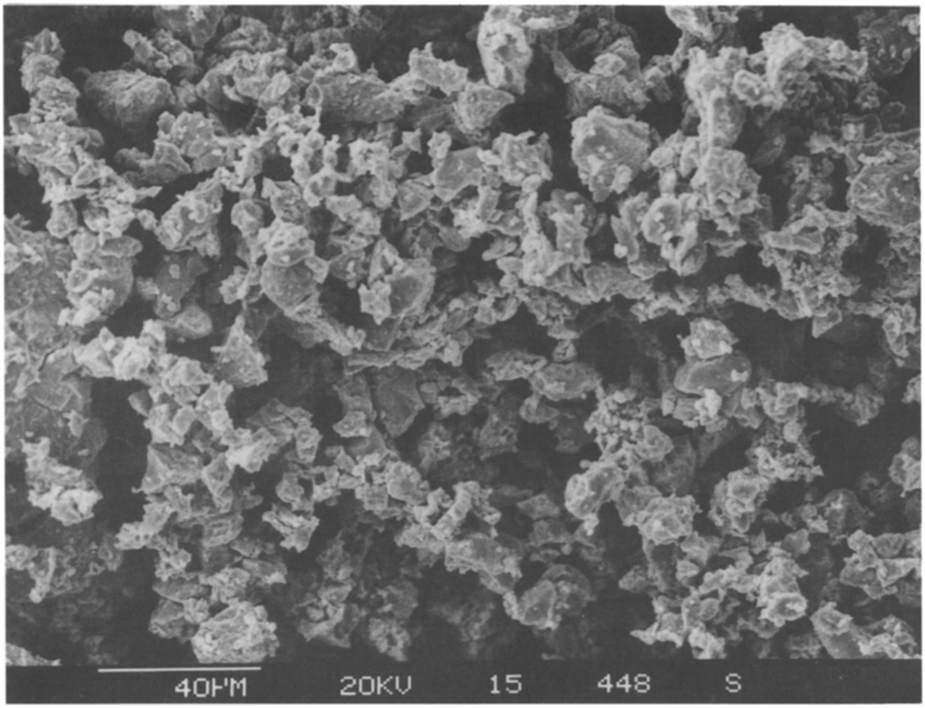

Fig. 11. SEM image of ZrH_2 powder.

longed reaction time is required. In case of the Ti(0)-catalyzed hydrogenation of zirconium sponge at 60°C in THF no latent period was observed.

A welcome benefit of the Ti(0)-catalyzed hydrogenation process is that the compact titanium and zirconium sponges break down during the H_2 uptake forming finely divided hydride powders. Fig. 11 shows the SEM image of a sample of ZrH_2 produced by catalytic hydrogenation of a zirconium sponge. The resulting 20 m powder has a very uniform size distribution.

X-ray diffraction of the products has provided an unambiguous identification of TiH_2 and ZrH_2. Protonolysis of the dry hydrides with 5 M HCl liberates 98% of the theoretically expected amount of H_2.

An interesting application of the Ti(0)-catalyzed metal hydrogenation process is the pressureless hydrogenation of a Ni/Zr/V/Ti/Cr alloy at room temperature. The corresponding hydride of this special alloy (Ni 38.2%, Zr 24.3%, Ti 12.8%, V 18.7%, Cr 6.0%) is of current interest for electrochemical purposes (nickel hydride battery). However, the hydrogenation at room temperature affords 5 bar hydrogen pressure and even under these conditions an unwanted latent period occurs. After doping the surface of the alloy with 1 wt.% of soluble Ti(0) using **3** as the precursor, a spontaneous uptake of 0.6–0.7 wt.% hydrogen is observed at room temperature without applying pressure.

Colloidal transition metals and alloys protected by tetraalkylammonium halides via reduction of metal salts with tetraalkylammonium hydrotriorganoborates

Based on the originally puzzling observation, that the reduction of noble metal chlorides, e.g. $PtCl_2$, with $NBu_4[BEt_3H]$ in THF besides giving the expected metal powders (Eqn. 6, Table 3) led to dark red solutions containing colloidal metals in THF, we were able to develop a general method for the preparation of metal colloids of elements of the groups 6–11 in the organic phase [11], [17]. The THF suspensions of the metal salts are treated with tetraalkylammonium hydrotriorganoborates, having alkyl groups preferentially of the chain lengths C_6–C_{20}. H_2 evolution occurs and brown–red metal colloid solutions are generated, from which only a small proportion of the reduced metal precipitates, Eqn. (14).

$$MX_\upsilon + \upsilon NR_{s4}(BEt_3H) \xrightarrow{THF} M_{colloid} + \upsilon NR_4X + \upsilon BEt_3 + \upsilon/2H_2\uparrow \qquad (14)$$

M = metal of groups 6–11, X = Cl, Br, $\upsilon = 1, 2, 3$, R = alkyl, C_6–C_{20}.

The long-chain tetraalkylammonium salts formed directly at the reduction centre in high local concentration act as very effective protecting agents to keep the particles of freshly reduced metal in solution (entropic stabilization factor). The filtered metal colloid solutions in THF resulting from Eqn. (14) are stable for months without any metal precipitation. In many cases the metal colloids have been isolated from the solution in the form of redispersible powders. The THF solutions are evaporated to dryness under high vacuum, the waxy residues are dissolved in ether, toluene or ethanol, and the metal colloid precipitated by addition of a third solvent (for details of the workup see Table 9 and Experimental). The resulting grey–black metal colloid powders may be

TABLE 9

Preparation of metal colloids in THF solution or as an isolated powder[a]

No.	Metal salt	Reducing agent	Conditions		Product colloid solutions colour	Work up solvent	Solvent added for precipitation	Metal content in isolated colloid (%)	Mean particle size (nm)
			t (h)	T (°C)					
1	MnI_2	$N(octyl)_4BEt_3H$	1	23	dark brown Mn completely dissolved				
2[b]	$FeBr_2$	$N(octyl)_4BEt_3H$	18	90	dark brown to black Fe almost completely dissolved	ethanol	ether	11.34	3.0
3	$RuCl_3$	$N(octyl)_4BEt_3H$	2	50	dark red-brown to black Ru almost completely dissolved	ethanol	pentane	68.72	1.3
4	$OsCl_3$	NBu_4BEt_3H	1	23	deep red to black				
5	$CoBr_2$	$N(octyl)_4BEt_3H$	16	23	dark brown to black Co completely dissolved	ethanol	ether	37.45	2.8
6	$RhCl_3$	$N(octyl)_4BEt_3H$	3	40	deep red to black Rh completely dissolved	ether	ethanol	73.40	2.1
7[a]	$IrCl_3$	$N(octyl)_4BEt_3H$	1	50	dark red to black Ir almost completely dissolved	ethanol	ether	65.55	1.5

8	$NiBr_2$	$N(octyl)_4BEt_3H$	16	23	dark red to black Ni completely dissolved	ethanol	ether	66.13	2.8
9	$NiBr_2$	$N(octyl)_3MeBEt_3H$	16	23	dark red to black Ni completely dissolved	ethanol	ether	68.29	2.8
10	$PdCl_2$	$N(octyl)_4BEt_3H$	1	23	dark brown to black Pd completely dissolved	ether	ethanol	83.62	2.5
11	$PtCl_2$	$N(hexyl)_4BEt_3H$	2	23	dark brown to black Pt up to 80% dissolved				
12	$PtCl_2$	$N(octyl)_4BEt_3H$	18	23	dark brown to black Pt completely dissolved	ether	ethanol	85.13	2.8
13	$PtCl_2$	$N(decyl)_4BEt_3H$	2	23	dark brown to black Pt up to 80% dissolved				
14	$CuCl_2$	$N(octyl)_4BEt_3H$	2	23	deep red to black Cu almost completely dissolved	ether	ethanol	77.04	
15	$CuBr_2$	$N(octyl)_4BEt_3H$	2	23	deep red to black Cu completely dissolved	toluene	ethanol	52.15	

[a]For a typical procedure see Experimental.

[b]Solvent: toluene.

redissolved in various organic solvents (e.g. ethers, hydrocarbons, esters) solubilities of up to 1 g at of metal per litre. Elemental analysis of the colloid powders and mass spectrometry indicate, that NR_4X is present. Presumably, the negatively charged metal core of the colloid is protected against agglomeration by the surrounding tetraalkylammonium ions (Fig. 12). This screening of the metal particles by large lipophilic alkyl groups explains the remarkable solubility of the colloids in organic solvents and their extraordinary stability.

The isolated metal colloids were examined by TEM. An inspection of the mean particle sizes quoted in Table 9 indicates that the metals form relatively small metal aggregates. In general the colloids prepared according to Eqn. (14) exhibit a narrow size distribution. Fig. 13 shows a typical particle size distribution determined from a TEM image of the Ir colloid (Table 9, No. 7).

HRTEM (high resolution transmission electron microscopy) of the Ir colloid (Table 9, No. 7) has further revealed, that surprisingly these small metal particles are crystalline (See the fringes in Fig. 14).

By coreduction of two different metal salts in analogy to Eqn. (14) the bimetallic colloids quoted in Table 10 have been prepared and isolated as redispersible powders. TEM images of the coreduction products show colloids with a narrow size distribution. Whether these bimetallic colloids (Table 10) are true colloidal metal alloys is under current investigation by the combination of X-ray diffraction, XPS, EXAFS, Mössbauer spectroscopy, and electrochemical studies. Fig. 15 shows the HRTEM image of the Pt/Rh coreduction product (Table 10, No. 1).

Metal particles of 2.3 nm size can be identified, showing net plane distances of 0.25 nm in the crystal. Under the microscope a number of particles were analyzed by EDX with a point resolution of 1 nm. Both Rh and Pt were

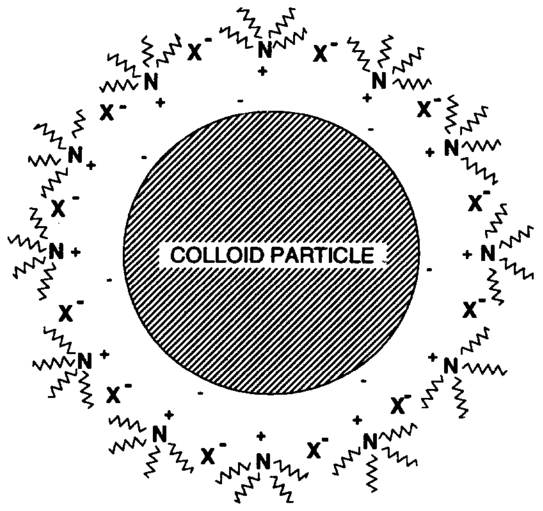

Fig. 12. Stabilization of the metal core with NR_4X.

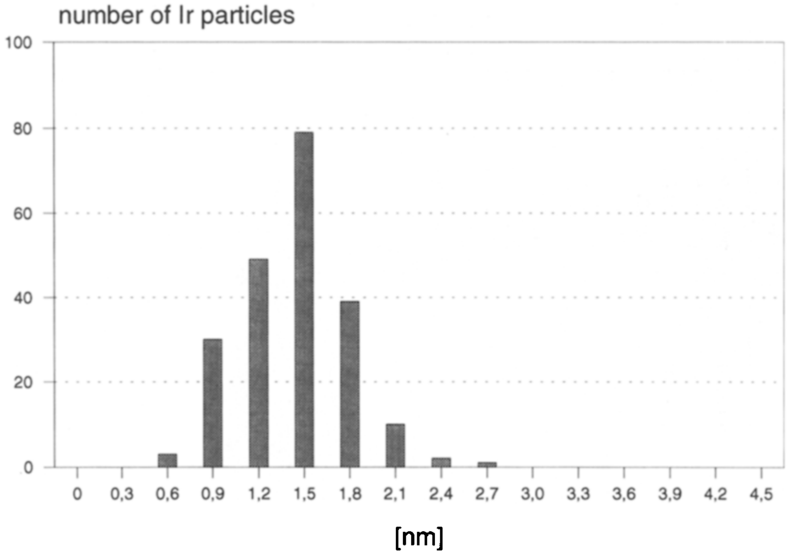

Fig. 13. Distribution of the particle size of Ir colloid (Table 9, No. 7).

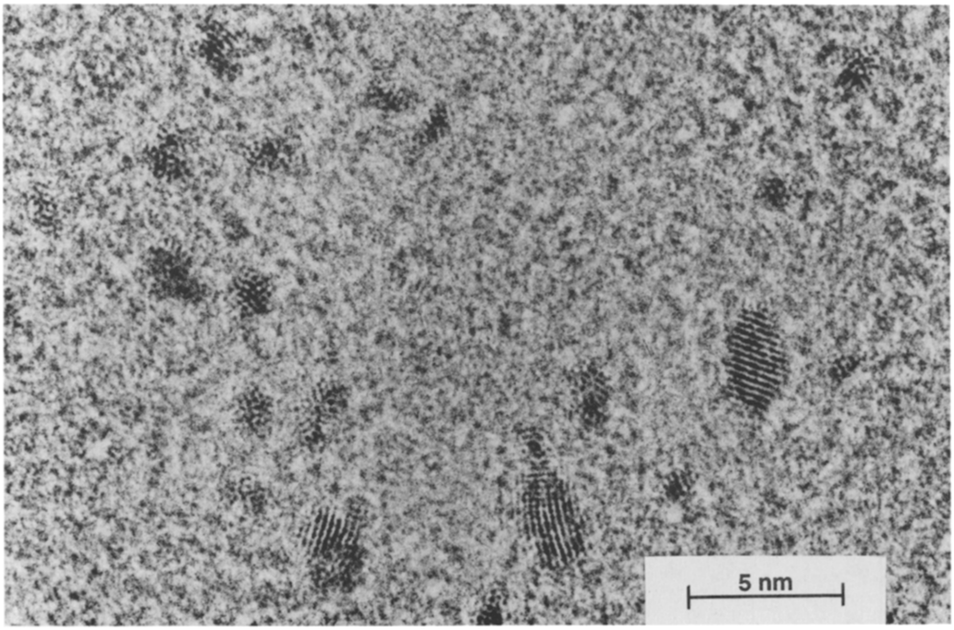

Fig. 14. HRTEM image of Ir colloid (Table 9, No. 7).

found to be present in every colloid particle examined. This result already indicates, that in fact a colloidal Pt/Rh alloy was obtained by the coreduction (Table 10, No. 1).

TABLE 10

Preparation of colloidal alloys [a]

No.	Metal salt	Reducing agent	Conditions		Colloidal alloy solution colour	Work up solvent	Solvent added for precipitation	Metal content in isolated colloid (%)	Mean particle size (nm)
			t	T (°C)					
1	$RhCl_3$ $PtCl_2$	$N(octyl)_4BEt_3H$	18	50	deep red to black Rh and Pt completely dissolved	ether	ethanol	Rh: 21.85 Pt: 45.96	2.3
2	$PdCl_2$ $PtCl_2$	$N(octyl)_4BEt_3H$	16	23	deep brown to black Pd and Pt completely dissolved	ether	ethanol	Pd: 25.9 Pt: 33.6	2.8
3	$CuCl_2$ $PtCl_2$	$N(octyl)_4BEt_3H$	16	23	deep red to black Cu and Pt completely dissolved	ether	ethanol	Cu: 15.6 Pt: 55.4	2.3
4	$PtCl_2$ $CoBr_2$	$N(octyl)_4BEt_3H$	18	23	deep redbrown to black Pt and Co completely dissolved	toluene	pentane/ethanol (25:1)	Pt: 25.4 Co: 6.47	-
5	$NiBr_2$ $CoBr_2$	$N(octyl)_4BEt_3H$	16	25	deep red to black Ni and Co completely dissolved	ethanol	ether	Ni: 23.8 Co: 23.8	2.8
6	$FeBr_2$ $CoBr_2$	$N(octyl)_4BEt_3H$	18	50	dark brown to black Fe and Co completely dissolved	ethanol	ether	Fe :13.36 Co :14.39	3.2

[a] Experimental procedure analogous Table 9, No. 2.

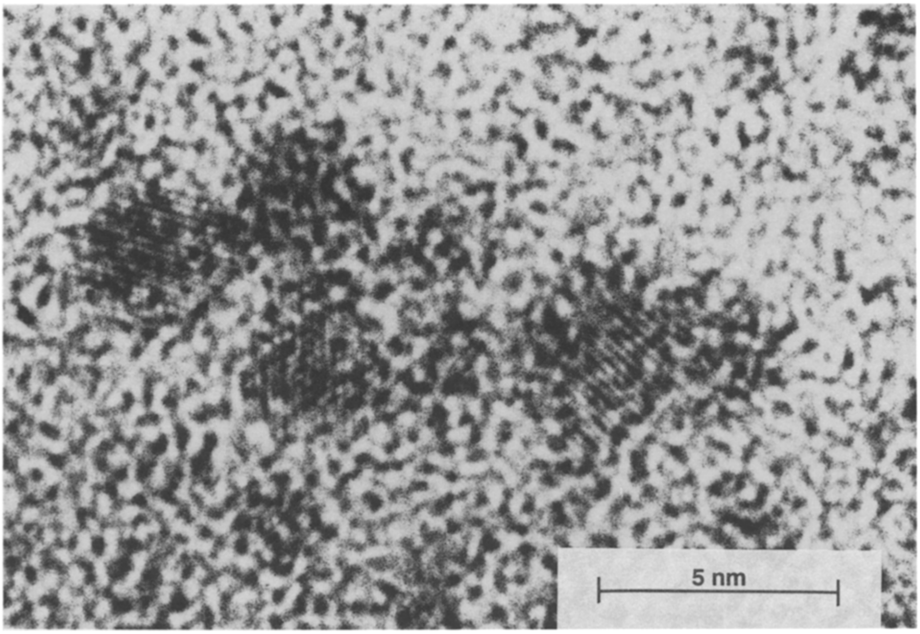

Fig. 15. HRTEM image of colloidal Pt/Rh alloy (Table 10, No. 1).

General approach to NR_4^+-stabilized metal colloids using conventional reducing agents [12]

In the synthesis, Eqn. (14), of colloidal transition metals discussed above, the stabilization of the metal particles was achieved by combining the stabilizing agent (NR_4^+) with the reducing agent ($NR_4[BEt_3H]$) in order to generate a high local concentration of stabilizing agent at the reduction centre (Entropic stabilization factor). A further development of this method led to NR_4^+ stabilized (isolable) metals of groups 6–11 by coupling the stabilizing agent to the metal salt which is to be reduced and reducing with simple inorganic and organic reducing agents (Eqn. 15).

$$(NR_4)_w MX_v Y_w + v\mathrm{Red} \rightarrow M_{\mathrm{colloid}} + v\mathrm{RedX} + wNR_4Y \qquad (15)$$

M: Metal of groups 6–11, Red: H_2, HCOOH, BEt_3, K, Zn, LiH, $LiBEt_3H$, $NaBEt_3H$, $KBEt_3H$ X, Y = Cl, Br, I, v, w = 1–3; R = C_6–C_{12}.

According to Eqn. (15) the disadvantage inherent in the use of a special reducing agent and the compulsory need of stoichiometric amounts of stabilizing agent in the original synthesis, Eqn. (14), may be avoided. The idea of coupling the stabilizing agent to the metal centre is exemplified for palladium: On the addition of $octyl_4NBr$ or $dodecyl_4NBr$ to a solution of $Pd(ac)_2$ in THF a strong colour intensification is observed which indicates the desired interaction between the Pd salt and the stabilizing agent. The NR_4^+ stabilized Pd colloid may now be obtained by simply bubbling hydrogen through the solution at room temperature. The optimal ratio of stabilizing agent to palladium is 1:2, which means that in comparison with the reduction using octyl$_4$NBEt$_3$H only about a quarter of the stabilizing agent is applied. This decrease in the amount of stabilizing agent facilitates the workup considerably.

Reduction of the NR_4^+ stabilized Pd(ac)$_2$ with hydrogen, formic acid, triethylborane or by thermal decomposition leads to stable palladium organo sols. By XPS examination of the Pd colloid quoted No. 9 in Table 11 the binding energies for the Pd 3d$_{5/2}$ and Pd 3d$_{3/2}$ electrons were found to be 334.3 eV and 339.3 eV respectively. Since the values theoretically expected for zero-valent Pd are 334.9 eV and 340.1 eV this result confirms that colloidal Pd(0) was produced in the reduction. Using the simplified preparation method, Eqn. (15), various noble and non-noble metal colloids have been obtained, which can be isolated in the form of redispersible powders by addition of protic solvents such as water or ethanol to the organic solution (Table 11). The mean particle size of the resulting colloids analyzed by TEM ranges from 0.5 nm in case of Ru (Table 11, No. 4) to a maximum of 4 nm found for palladium (Table 11, No. 13).

The stabilizing agent (e.g. octyl$_4$NBr) can also be attached to the metal in the form of a defined tetraalkylammonium metalate. Esumi [28], Blum and others [36] have introduced solvent–solvent extractions using tetraalkylammonium salts to transfer noble metal halides from aqueous HCl into organic solvents. We, however, dissolve e.g. palladium, platinum, and nickel halides in THF simply by heating with tetraalkylammonium halides (Eqn. (16)).

$$PdX_2 + 2NOctyl_4Y \xrightarrow[THF]{16\ h,\ reflux} (NOctyl_4)_2PdX_2Y_2 \qquad (16)$$

For the success of the reductive colloid synthesis from the corresponding metalates, Eqn. (16) the choice of an appropriate anion is important: The reduction of (octyl$_4$N)$_2$PdCl$_4$ with hydrogen gives a metallic precipitate and (octyl$_4$N)$_2$PdBr$_4$ is not reduced even under 50 bar hydrogen atmosphere. From (octyl$_4$N)$_2$PdCl$_2$Br$_2$, however, a palladium colloid showing a narrow size distribution [12] was obtained (Table 11, No. 13).

The preparation of bimetallic colloids by coreduction of different metal salts according to this concept is also successful. Currently we are continuing to investigate this promising subject.

Nanoscale metal powders via metal colloids

The fact that neither halogen nor nitrogen could be detected in the EDX spectra of the colloid particles under UHV (ultra high vacuum) conditions in the electron microscope column or by XPS at ca. 150°C and 10^{-7} to 10^{-8} Pa clearly indicates that the protecting teraalkylammonium halide may be removed under certain conditions leaving the bare metal core behind. This observation prompted us to develop a chemical procedure for the careful extraction of the protecting shell at room temperature in order to produce nanoscale

TABLE 11

Preparation of NR_4^+ stabilized metal colloids using conventional reducing agents [a]

No.	Precursor	Reducing agent	Conditions		Solvent	Metal content in isolated colloid (%)	Mean particle size (nm)
			t	*T* (°C)			
1	$[N(octyl)_4]_2NiBr_4$	K	72 h	22	THF	57	2.8
2	$CoBr_2 \cdot 2N(octyl)_4Br$	$NaBEt_3H$	72 h	22	THF	31	2.8
3	$CoBr_2 \cdot 2N(octyl)_4Br$	K	72 h	22	THF	32	2.8
4	$RuCl_3 \cdot 3N(octyl)_4Br$	$KBEt_3H$	16 h	22	THF	-	0.5
5	$RhCl_3 \cdot 3$Aliquat 336	H_2 (50 bar)	4 h	22	THF	74	3.0
6	$RhCl_3 \cdot 3N(octyl)_4Br$	$LiBEt_3H$	16 h	50	THF	-	2.1
7	$RhCl_3 \cdot 3N(octyl)_4Br$	LiH	16 h	60	THF	-	2.1
8	$RhCl_3 \cdot 3N(octyl)_4Br$	Zn	16 h	60	THF	-	2.2
9[a]	$Pdac_2/N(dodecyl)_4Br$	H_2	16 h	22	THF	77	1.8
10	$Pdac_2/N(dodecyl)_4Br$	HCOOH	16 h	60	THF	73	1.8
11	$Pdac_2/N(dodecyl)_4Br$	BEt_3	8 days	22	THF	71	2.5
12	$Pdac_2/N(dodecyl)_4Br$	–	3 h	125	*p*-xylene	86	2.1
13	$[N(octyl)_4]_2PdCl_2Br_2$	H_2	14 days	22	THF	-	4.0
14	$[N(octyl)_4]_2PtCl_2Br_2$	$LiBEt_3H$	1 h	22	THF	-	1.9

[a] For a typical procedure see Experimental, Aliquat 336 = trioctylmethylammonium chloride.

metal powders from the colloids shown in Table 9 and 10. This is exemplified with nanoscale platinum powder prepared from the corresponding platinum colloid (Table 9, No. 12): In order to extract the stabilizing tetraalkylammonium halide the grey–brown colloid powder is treated with excess ethanol. The supernatant solution of the tetraalkylammonium halide is siphoned and subsequently the colour of the product darkens. After several repetitions a pyrophoric metal powder (93% Pt) is obtained which is no longer redispersible in THF (Table 12, No. 5). The TEM image of this product (Fig. 16) shows that the mean particle size of the platinum powder found after the extraction corresponds exactly to the particle size of the colloidal platinum which was used as the starting material. However, small residues of the protecting shell are still present in the sample. Interestingly, this contaminations can be completely removed by an after-treatment of the metal powder at 700°C and 0.1 Pa. An inspection of the TEM image of the product (Fig. 17) proves, that the original particle size of the colloidal platinum (2.8 nm) was conserved and no unwanted agglomeration of the nanoparticles is observed as a consequence of the heat treatment.

This finding has successfully been exploited for the preparation of various nanoscale metal and alloy powders via metal colloids (Table 12). According to TEM as a rule the particle size of the metal and alloy powders obtained corresponds to the size found in the colloidal starting material. The only exception was found so far with palladium, where the removal of the protecting shell caused an augmentation of the particles from 2.5 nm to 6.0 nm. After the heat treatment, however, the size of the palladium nanoparticles remained unchanged.

Catalytic applications

Metal colloids may be useful as homogeneous and heterogeneous hydrogenation catalysts. In the homogeneous phase the activities of different palladium colloids were determined by the hydrogenation of cyclohexene in THF under standard conditions [12] (See Experimental). The adsorption of the noble metal colloids on charcoal gave standard samples of heterogeneous catalysts covered with 5% Pd [12], 5% Rh [34] or 5% Pt which were tested in the hydrogenation of cinnamic acid, butyronitrile or crotonic acid respectively. These standard substrates are routinely applied for commercial industrial catalysts (See Experimental). Fig. 18 shows the set-up used for determining the maximal catalyst activity. As the highest activity is found at the start of the reaction, this apparatus was used for short time tests. The central element is a thermostatically controlled standard test reactor which is directly compatible with an industrial testing apparatus used for catalyst quality control. The agitated vessel reactor is evacuated to a residue pressure of 10 Pa via the vacuum pump (c) and then backfilled with hydrogen. The catalyst is flushed into the reactor using solvent from the reservoir (d). The substrate is introduced by injection through a septum (e) initiating the reaction. The reaction mixture

TABLE 12

Preparation of nanoscale metal powders via metal colloids[a]

No.	Starting material		Solvent for extraction of NR_4X	Product metal contecnt after extraction (%)	Mean particle size	
	Colloid	Mean particle size (nm)			After extraction (nm)	After heat treatment (7900°C, 4h, 10^{-3} mbar) (nm)
1	Co Table 9, No. 5	2.8	ethanol	82.84	3.8	-
2	Ni Table 9, No. 8	2.8	ethanol	88.18	3.0	-
3	Rh Table 9, No. 6	2.1	ethanol	82.76	2.7	2.9
4	Pd Table 9, No. 10	2.5	ethanol	98.13	5.8	6.0
5[a]	Pt Table 9, No. 12	2.8	ethanol	92.90	2.8	2.8
6	Rh/Pt Table 10, No. 1	2.3	ether/ethanol 1:10	-	2.7	3.0
7	Pd/Pt Table 10, No. 2	2.8	ether/ethanol 1:10	-	2.8	-

[a] For a typical procedure see Experimental.

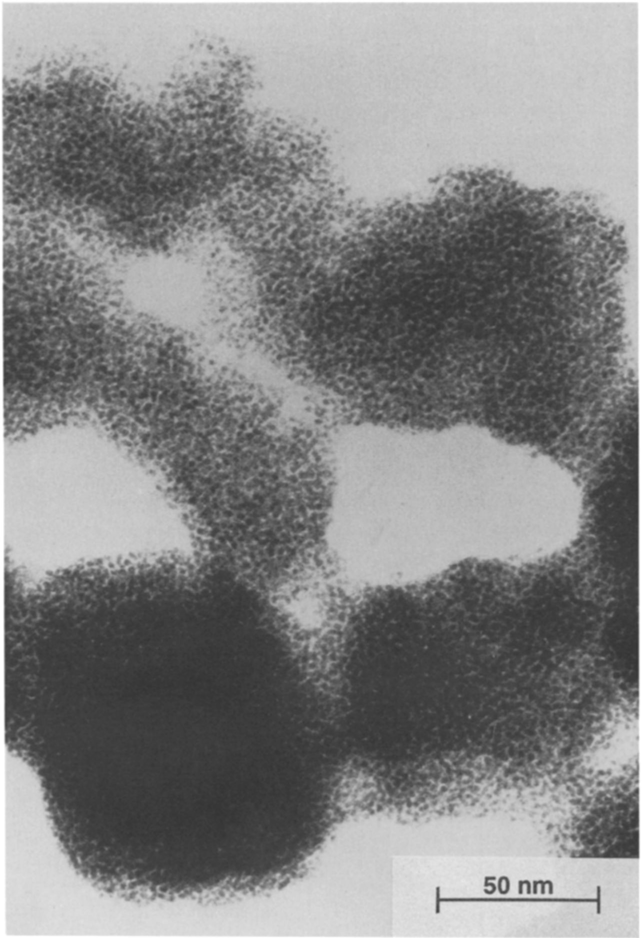

Fig. 16. TEM image of Pt powder obtained from Pt colloid (Table 12, No. 5).

is agitated using a self aspirating hollow stirrer (f) to achieve an intimate mixture between the suspension and the gas phase. During the catalysis the hydrogen supply is provided by one of the two gas burettes (g, h). The 900 ml burette is connected to a 2 channel recorder (j) via a displacement-voltage recorder (i). This registers the amount of hydrogen consumed and the reaction temperature at the thermocouple (k) and the digital thermometer (l).

Based on the hydrogen consumption in the first five minutes, the activity of the catalyst is calculated in terms of [N ml/(g min)]. In order to investigate the selectivity, a sample is taken at the end of the experiment and the reaction products are identified by GC. Besides activity, the stability (lifetime) of the catalyst is of particular interest. This is tested in a second reactor unit. With respect to the experimental set up described in Fig. 18, the main difference here concerns the hydrogen supply. Since a greater amount of gas is needed

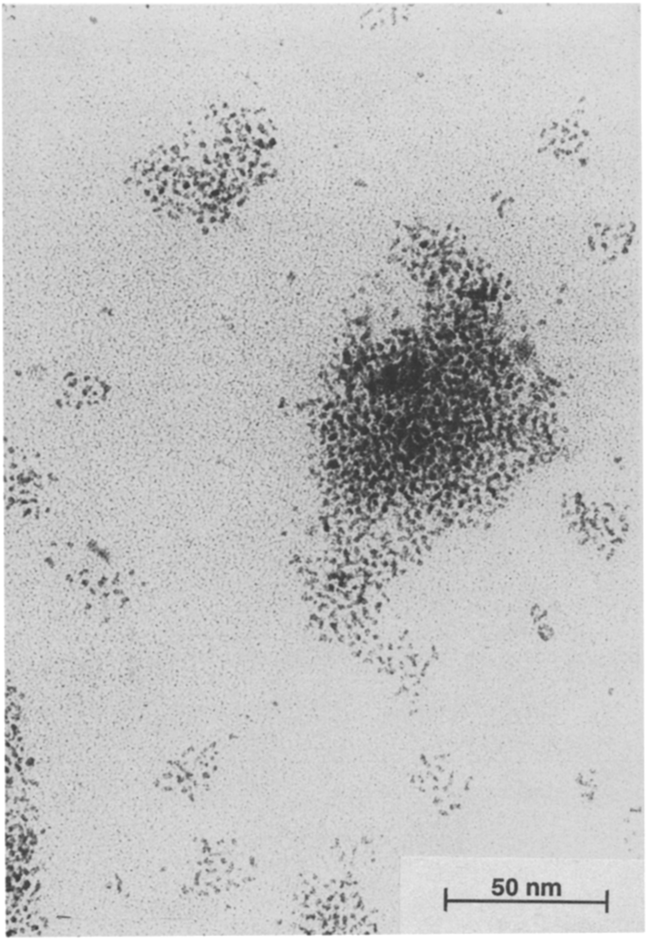

Fig. 17. TEM image of Pt powder obtained from Pt colloid (Table 12, No. 5) after thermal treatment (4h, 700 °C, 0.1 Pa).

during the stability test, additional hydrogen is supplied automatically from a 200 ml stainless steel autoclave through a reducing pressure valve. The pressure drop in the autoclave, registered on a 2 channel recorder, is proportional to the amount of hydrogen consumed.

Free and supported metal colloid catalysts in liquid-phase hydrogenation

The free nickel and palladium colloids are suitable for the selective hydrogenation of naturally occurring products such as soya bean oil. Table 13 summarizes the activities of various palladium colloids in the homogeneous cyclohexene hydrogenation.

An inspection of Table 13 reveals that neither the method used for the preparation (Eqn. 14 or 15) nor the particle size of the colloid has a systematic

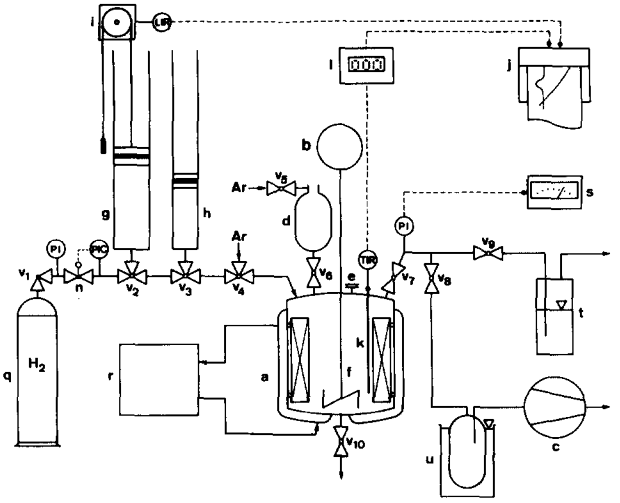

a	reactor
b	stirrer drive
c	vacuum pump
d	condensate tank
e	septum
f	self-aspirating hollow stirrer
g	900 ml gas burette
h	200 ml gas burette
i	displacement voltage converter
j	2 channel recorder
k	thermocouple
l	digital thermometer
n	reducing pressure valve
q	H_2 - gas cylinder
r	thermostat
s	pressure reading
t	bead vessel
u	cold trap
v1 - v10	fittings:
⋈	two-way cock
⋈	three-way cock
⋈	through way valve
⋈	(right) angle valve
---	signal flow

Fig. 18. Apparatus for the determination of the catalyst activity.

TABLE 13

Anion dependent activity of colloidal palladium in the homogeneous cyclohexene hydrogenation test [a]

No.	Catalyst	Preparation method for the colloid	Particle size (nm)	Activity (N ml/g min)
1	$PdBr_2/N(octyl)_4BEt_3H$	similar to Table 9, No.10	-	1169
2	$PdCl_2/N(octyl)_4BEt_3H$	Table 9, No.10	2.5	479
3	$Pdac_2/N(octyl)_4BEt_3H$	similar to Table 9, No.10	2.9	241
4	$PdI_2/N(octyl)_4BEt_3H$	similar to Table 9, No.10	-	0
5	$N(octyl)_4PdCl_2Br_2/H_2$	Table 11, No.13	4.0	762
6	$Pdac_2\cdot 2N(dodecyl)_4Br/H_2$	Table 11, No.9	1.8	377

[a] See Experimental.

influence on the resulting catalytic activity. Surprisingly, the choice of the anion is found to be important. In the order of Br > Cl > ac > I a strong decrease in the catalytic activity of the colloidal palladium in the cyclohexene test was observed. A major disadvantage of the free colloids, however, lies in the tendency of non-supported hydrogenation catalysts to agglomerate very easily in solution which causes metal precipitation and consequently prompts a drastic loss of activity. In the case of the free colloidal palladium catalysts the first metal precipitation already occurs after 6–7 minutes. Adsorption of the metal colloids onto technically important supports such as charcoal improves the stability of the resulting catalysts substantially. In contrast to a widespread prejudice it was found that the catalytic activity is not deteriorated automatically when the metal particles are supported: Table 14 compares the activity values measured with free colloidal palladium and supported on charcoal (5%

TABLE 14

Comparison of the catalytic activity of a colloid-free or supported (5% on C)[a] palladium catalyst

No.	Catalyst	Preparation method for the coloid	Support	Solvent	Substrate	Activity (N ml/g min)
1	$PdCl_2/N(octyl)_4BEt_3H$	Table 9, No.10	-	THF	cyclohexene[b]	479
2	$PdCl_2/N(octyl)_4BEt_3H$	Table 9, No.10	charcoal	THF	cyclohexene	566
3	$PdCl_2/N(octyl)_4BEt_3H$	Table 9, No.10	-	THF	cinnamic acid[b]	329
4	$PdCl_2/N(octyl)_4BEt_3H$	Table 9, No.10	charcoal	THF	cinnamic acid	207

[a]Based on the weight of Pd used.
[b]For the test procedure see Experimental.

TABLE 15

Catalytic activity of supported colloidal palladium (5% Pd on C) in the cinnamic acid test[a]

No.	Catalyst	Colloid precursor	Activity (N ml/g min)
1	Pd on C (Degussa E 10 R/D)[b]	-	356
2	$PdCl_2/N(octyl)_4BEt_3H$ on C	Table 9, No. 10	406
3	$N(octyl)_4PdCl_2Br_2/H_2$ on C	Table 11, No. 13	826
4	$Pdac_2/N(dodecyl)_4Br$/on C	Table 11, No. 9	586
5	$Pdac_2/N(dodecyl)_4Br/HCOOH$ on C	Table 11, No. 10	401
6	$Pdac_2/N(dodecyl)_4Br/BEt_3$ on C	Table 11, No. 11	389
7	$Pdac_2/N(dodecyl)_4Br$[c] on C	Table 11, No. 12	310

[a]See Experimental.
[b]Precipitation of Pd on C.
[c]Thermal decomposition at 125°C.

Pd/C). Both in the cyclohexene test (Table 14, Nos. 1 and 2) and in the cinnamic acid test (Table 14, Nos. 3 and 4) only minor differences in the catalytic activity of the free and supported palladium colloid were found. (Because the free palladium colloid is insoluble in ethanol the cinnamic acid test had to be performed in THF for comparison. For the standard activity of 5% Pd/C in ethanol see Table 15, No. 2).

These findings were confirmed by a comparison of the mean particle size in the TEM images of the palladium colloid (Table 11, No. 13) in the free and supported form used in the catalytic test reactions quoted in Table 14. The free colloid is shown in Fig. 19 (left side). As shown in Fig. 19 (right side) the mean particle size of the free precursor (4.0 nm) remains virtually unchanged by the adsorption process; the dispersion of the palladium colloid on the charcoal appears to be remarkably uniform. This effect is probably due to the fact that the discrete particles in the free colloid (Fig. 19, left) are well separated from each other by the long chain hydrocarbon groups present in the tetraalkylammonium protecting shell. As a consequence, an unwanted agglomeration of the

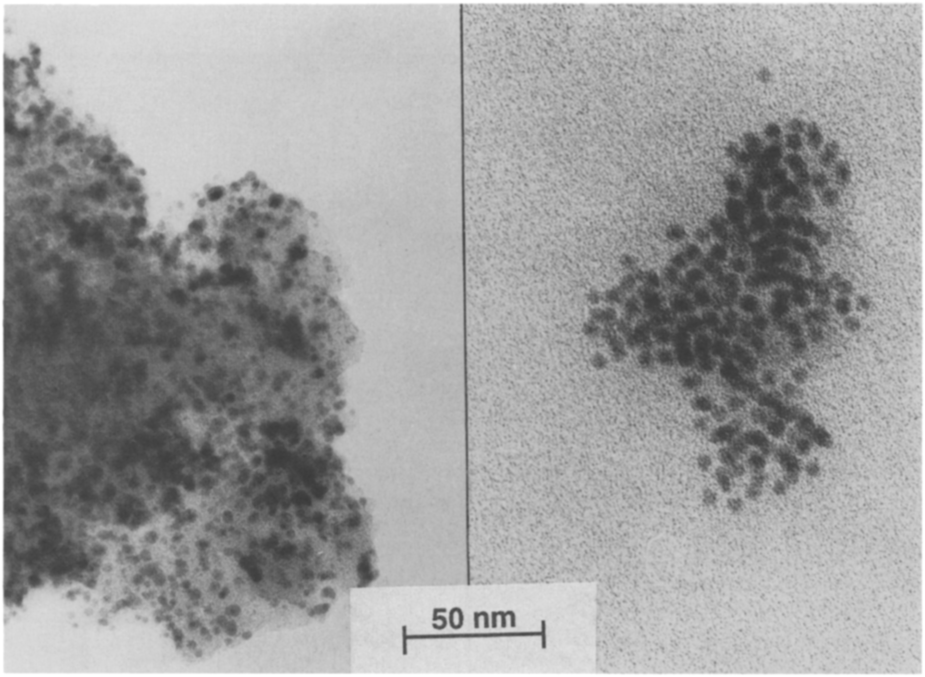

Fig. 19. TEM image of Pd colloid (Table 11, No. 13) (left) free, and (right) supported on charcoal.

metal cores on the support surface is prevented. The conservation of the particle size of the metal colloids after the adsorption was further checked by analogous TEM images of free and supported colloidal rhodium [34].

The activities (cinnamic acid test) of supported Pd/C catalysts (Table 15, Nos. 2, 5, 6, 7) prepared on the basis of the colloids quoted in Table 9, No. 10 and Table 11, Nos. 10, 11, and 12 are comparable to the industrial catalyst (Table 15, No. 1). Substantially higher activities are observed in case of the Pd/C catalysts (Table 15, Nos. 3 and 4) prepared from the colloids in Table 11, Nos. 9 and 13. In case of the supported colloid (Table 15, No. 3) the activity was enhanced by a factor of 2.3 in comparison to the conventional catalyst (Table 15, No. 1).

The activities of colloidal platinum catalysts (5% supported on charcoal) in the crotonic acid test are compared in Table 16 with a conventional 5% Pt/C catalyst prepared by the precipitation method. The Pt/C catalyst No. 3 prepared from the isolated platinum colloid (Table 11, No. 14) exceeds the activity of the conventional catalyst. As can be seen by comparison (Table 16, Nos. 2 and 3), the crude platinum colloid solution can be adsorbed directly from the reaction batch on charcoal without affecting the activity of the resulting catalyst. A TEM image of the industrial Rh/C catalyst (Table 16, No. 5), conventionally prepared by precipitation of aqueous $RhCl_3$ on charcoal, has re-

TABLE 16

Catalytic activity of supported colloidal platinum and rhodium (5% on C)

No.	Catalyst	Colloid precursor	Substrate	Activity (N ml/g min)
1	Pt on C (Degussa F 103 R7D 314)[a]	-	crotonic acid[b]	254
2	$PtCl_2/N(octyl)_4BEt_3H$ on C	Table 9, No.12 reaction solution	crotonic acid	387
3	$PtCl_2/N(octyl)_4BEt_3H$ on C	Table 9, No.12 isolated colloid	crotonic acid	415
4	$[N(octyl)_4]_2PtCl_2Br_2/LiBEt_3H$ on C	Table 11, No.14	crotonic acid	258
5	Rh on C (Degussa G 10 S)[a]	-	butyronitrile[b]	71
6	$RhCl_3/N(octyl)_4BEt_3H$ on C	Table 9, No.6	butyronitrile	95

[a] Precipitation on C.
[b] For the test procedure see Experimental.

vealed that only minor parts of the metal are well dispersed on the surface [34]. In contrast, the adsorption of the pre-prepared rhodium colloid (Table 9, No. 6) on charcoal was shown to yield a remarkably uniform metal dispersion on the charcoal with full conservation of the particle size found in the colloidal precursor [34]. Consequently the activity in the butyronitrile test of the conventional Rh/C catalyst is surpassed by 33% by the rhodium colloid supported on charcoal (Table 16, Nos. 5 and 6).

For reasons of comparison both the conventional Rh/C catalysts and the rhodium colloid/C systems were prepared under argon. In order to obtain air stable products, we have treated the ready-made dry catalysts carefully for 2 h with argon that contained 0.2 vol% molecular oxygen [34]. We were surprised to find that the careful oxygenation of the surface not only stabilizes both types of catalysts to air, but also considerably enhances their activity. In the case of the conventional Rh/C catalyst the oxygenation step improves the activity by 17% (Table 17, Nos. 1 and 2). The more active rhodium colloid/C catalyst (Table 17, No. 4) approximately doubles its activity after oxygenation (Table 17, No. 6). These findings are in good correspondence with a report published by Willstätter as early as 1921 [37], concluding that the activity of noble-metal hydrogenation catalysts is strongly oxygen dependent.

Using TiO_2 as a carrier for noble metal hydrogenation catalysts, most effective strong metal support interactions (SMSI) have been reported [38] [39]. Ryndin et. al. [40] systematically investigated the effect of early transition metal ions as dopants for noble metal hydrogenation catalysts on neutral supports such as silica or graphite. The tetravalent titanium, zirconium, and hafnium ions were reduced on the support by thermal after-treatment under hydrogen. However, using zero-valent titanium in the form of bis(arene)Ti(0) compounds or $[Ti(0) \cdot 0.5THF]_x$ as dopants at room temperature without further thermal treatment or hydrogenolysis, we have observed that the catalytic

TABLE 17

Effect of dopant and oxygenation on the catalytic activity of precipitated and colloidal rhodium (5%) on C in the butyronitrile test [a]

No.	Catalyst	Preparation method	Dopant	Oxygenated	Activity (N ml/g min)	Enhancement (%)
1	Rh on C	conventional precipitation under Ar [b]	-	–	71	standard
2	Rh on C	conventional precipitation under Ar	-	+	83	17
3	Rh on C	conventional precipitation under Ar	0.2% Ti(toluene)$_2$ [c]	+	124	75
4	$RhCl_3/N(octyl)_4BEt_3H$ on C	colloid (Table 9, No.6) adsorbed	-	–	95	34
5	$RhCl_3/N(octyl)_4BEt_3H$ on C	colloid (Table 9, No.6) adsorbed	0.2% Ti(toluene)$_2$	–	123	73
6	$RhCl_3/N(octyl)_4BEt_3H$ on C	colloid (Table 9, No.6) adsorbed	-	+	203	186
7	$RhCl_3/N(octyl)_4BEt_3H$ on C	colloid (Table 9, No.6) adsorbed	0.2% Ti(toluene)$_2$	+	262	269
8	$RhCl_3/N(octyl)_4BEt_3H$ on C	colloid (Table 9, No.6) adsorbed	0.2% $[Ti \cdot 0.5\ THF]_x$ [d]	+	263	270

[a] See Experimental.

[b] [34].

[c] For Experimental see [34].

[d] For Experimental see [41].

activity of Rh/C catalysts in the butyronitrile test may be considerably enhanced [34,41]. A comparison of the activity figures quoted in Table 17 shows that doping of the supported rhodium colloid catalyst with 0.2% Ti(0) is most effective in combination with subsequent oxygenation.

The long-time stability of conventional and colloidal noble metal catalysts on charcoal was tested by measuring the total turnover number of the systems in the hydrogenation of cyclooctene in ethanol at 40° C. This is exemplified in Fig. 20 for the industrial Pd/C catalyst (Table 15, No. 1) and the supported palladium colloid catalyst (Table 15, No. 3). Whereas the activity of the conventional precipitation catalyst expires completely after the performance of 38×10^3 catalytic cycles per palladium atom, the colloidal Pd/C catalyst still shows a residual activity of 30 N ml H_2/(g min) after 96×10^3 catalytic turnovers. However, the superiority of the colloidal system over the conventional catalyst observed for palladium in this case cannot be generalized.

The hydrogenation activity of the supported bimetallic Pt/Rh colloid (cf. Table 10, No. 1) (5% metal on C) was investigated using the crotonic acid test. In order to elucidate the cocatalytic influence of rhodium, the activity of the bimetallic systems was plotted against increasing amounts of rhodium present in various Pt/Rh colloids adsorbed on charcoal (Fig. 21, curve 1). For comparison, samples of platinum colloid (Table 9, No. 12) were mixed in solution with increasing amounts of rhodium colloid (Table 9, No. 6) and then adsorbed at charcoal (5% metal). The activities of the resulting catalysts in the crotonic acid test were plotted against the Pt/Rh ratio in Fig. 21, curve 2. Further, samples of the ready-made Pt/C catalyst (Table 16, No. 2) were thoroughly mixed with increasing amounts of the corresponding Rh/C catalyst (Table 16, No. 6); the resulting activity values, plotted against the Pt/Rh ratio are shown in Fig. 21, curve 3.

Whereas the catalysts prepared by mixing Pt/C and Rh/C (curve 3) or

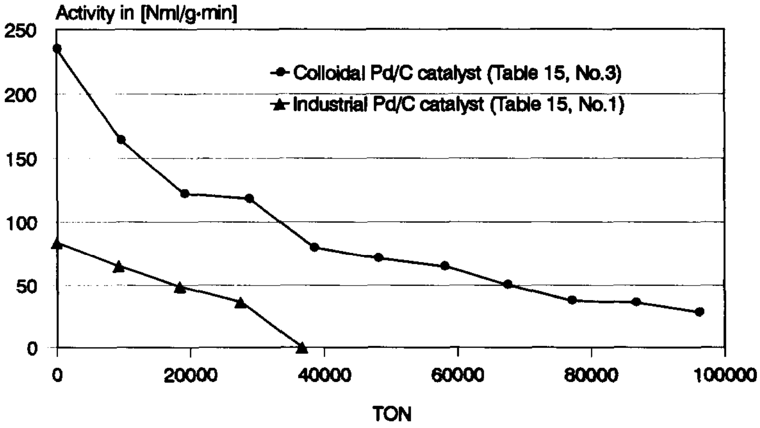

Fig. 20. Stability of Pd/C catalysts in the hydrogenation of cyclooctene.

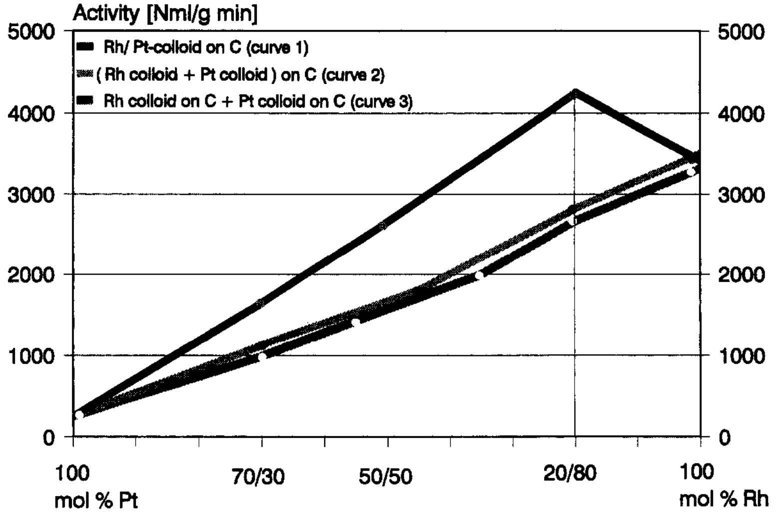

Fig. 21. Activity plot of the Rh/Pt bimetallic system in comparison to mixed Pt and Rh catalysts. X, Y = Cl, Br.

by supporting mixtures of separately made platinum and rhodium colloid samples on charcoal (curve 2) clearly show a linear increase of the activity with increasing content of rhodium (additive effect of platinum and rhodium), the corresponding activity plot of the bimetallic Pt/Rh systems (curve 1) exhibits a maximum at $Pt_{20}Rh_{80}$. This obviously accounts for a synergistic effect of the two metals in the bimetallic colloid at certain atomic ratios which may be interpreted as a further indication that a Pt/Rh alloy colloid was present in the precursors formed by coreduction (cf. Table 10, No. 1 and Fig. 15).

Conclusions

The results presented here establish that metals and metal alloys of 10–100 nm particle size are easily accessible through the chemical reduction of metal salts or metal oxides with of hydrotriorganoborates. Transition metal colloids (1–10 nm), including bimetallic colloids, stabilized by NR_4X may be prepared similarly. These materials are of special interest with respect to alloy formation and segregation processes. Furthermore, they have been shown to be active catalysts both in the homogeneous and heterogeneous phase. The noble metal colloids may be deposited on surfaces with an unusually high degree of dispersion. The pretreatment of the support with low-valent titanium considerably enhances the catalytic activity in liquid-phase hydrogenations. Bimetallic Pt/Rh colloid catalysts show a higher activity compared with a combination of the individual metals. These observations, together with the structural characterization of the particles by physical methods, open promising perspectives for catalyst design.

Experimental

All reductions using metals or hydrides were carried out under argon in dry solvents. For conventional reductions using e.g. H_2 commercial starting materials and solvents of technical quality were used.

Preparation of finely divided metal and alloy powders from metal salts

Preparation of nickel powder from Ni(OH) and Na[BEt$_3$H] in THF

A solution of 5 g (41 mmol) of $Na[BEt_3H]$ dissolved in THF (1 molar) was added dropwise at 23°C to a stirred suspension of 1.85 g (20 mmol) $Ni(OH)_2$ in 200 ml of THF in a 500 ml flask. After 2 h the clear reaction solution was washed with 200 ml aliquots of THF, ethanol, THF and pentane successively. After drying under high vacuum (0.1 Pa), 1.15 g of metal powder was obtained: metal content: Ni 94.7%; BET surface area: 29.7 m^2/g.

Preparation of Na[(Et$_2$GaOEt)H]

A solution of 34.5 g (200 mmol) of diethylethoxygallium – Et_2GaOEt – was boiled under reflux in 400 ml of THF with 30.5 g (1270 mmol) of NaH for 4 h. A clear solution was obtained from which excessive NaH was removed by filtration using a D-4 glass frit. A 0.45 M solution was obtained as ascertained by protonolysis with ethanol.

Preparation of palladium powder from PdCl$_2$ and Na[(Et$_2$GaOEt)H]

A solution of 45 ml (20.25 mol) of the $Na(Et_2GaOEt)H$ thus obtained was added dropwise at 40°C to a stirred suspension of 1.91 g (10.76 mmol) of $PdCl_2$ in 200 ml of THF in a 500 ml flask. After 2 h the palladium powder was filtered from the clear reaction solution. Then the palladium powder was washed twice with 200 ml portions of H_2O, THF, and pentane. After drying under high vacuum (0.1 Pa), 1.2 g of metal powder was obtained: metal content: Pd 92.7%.

Preparation of platinum powder from PtCl$_2$ and Li[BEt$_3$H] in THF

A solution of 4.24 g (40 mmol) of $Li[BEt_3H]$ dissolved in THF (1 molar) was added dropwise at 65°C to a stirred suspension of 4.0 g (15 mmol) of $PtCl_2$ in 250 ml of THF in a 500 ml flask. After 12 h the clear reaction solution was separated from the platinum powder. Then the platinum powder was washed with 200 ml aliquots of THF, ethanol, THF, and pentane successively. After drying under high vacuum (0.1 Pa), 2.80 g of metal powder was obtained: metal content: Pt 99.0%.

Preparation of an iron–cobalt alloy from FeCl$_3$, CoCl$_2$ and Li[BEt$_3$H] (cf. Figs. 3, 4 and 5)

A solution of 9.1 g (56 mmol) of $FeCl_3$ and 3.1 g (24 mmol) of $CoCl_2$ in 2.5 l of THF was added dropwise to a stirred 1.7 M (255 mmol) solution of

Li[BEt_3H] in THF over 5 h at 23 °C. After stirring overnight, the iron cobalt alloy was filtered off from the clear reaction solution and washed twice with 200 ml portions of THF. The product was then stirred with 300 ml of ethanol and subsequently with a mixture of 200 ml of ethanol and 200 ml of THF until the gas evolution ceased. Finally, the product was washed again with 2×200 ml of THF. The yield of alloy powder after drying under high vacuum (0.1 Pa) was 5.0 g. Metal content: Fe 64.40%; Co 31.60%. X-ray diffractogram: (measured with CoK_α radiation, Fe filter); strongest reflection 2Θ: 52.7°; lattice spacing of planes, *d*: 2.02 Å.

Preparation of a palladium platinum alloy from $PdCl_2$, $PtCl_2$ and Li[BEt_3H]

A solution of 5.3 g (50 mmol) of Li[BEt_3 H] dissolved in 50 ml of THF was added dropwise with stirring to a refluxed suspension of 1.77 g (10 mmol) of $PdCl_2$ and 2.66 g (10 mmol) of $PtCl_2$ in 250 ml of THF in a 500 ml flask. After 5 h the mixture was allowed to cool to 23 °C, and the alloy powder filtered off and washed with 250 ml aliquots of THF, ethanol, THF, and pentane successively. The yield of alloy powder after drying under high vacuum (0.1 Pa) was 3.02 g. Metal content: Pd 33.6%; Pt 63.4%; boron content: 0.04%. X-ray diffractogram (measured with CoK_α radiation, Fe filter): strongest reflections 2Θ: 40.1° (46.3°); lattice spacing of planes, *d*: 2.25 Å (1.96 Å).

Preparation of platinum powder from $PtCl_2$ and Na[BEt_3H] in THF

A solution of 6.71 g (55 mmol) of Na[BEt_3H] dissolved in THF (1 molar) was added dropwise at 23 °C with stirring to a suspension of 2.5 g (10.9 mmol) of $PtCl_2$ in 100 ml of THF in a 250 ml flask. The clear reaction solution was separated from the platinum powder after 2 h, and the latter was washed with 100 ml aliquots of THF, ethanol, THF, and pentane successively. The yield of metal powder after drying under high vacuum (0.1 Pa), was 2.05 g.

Preparation of metal and alloy powders from metal oxides

Preparation of iron pigment from FeOOH, Na[BEt_3H] and H_2 in toluene (cf. Figs. 6 and 7)

In a 5 l autoclave equipped with a stirrer, 96 g (1.078 mol) of FeOOH under a protective gas was admixed with 1.22 l of a 2.67 M solution of Na[BEt_3H] in toluene and filled up with toluene to a working volume of 3.0 l. H_2 was added at room temperature to a pressure of 100 bar, and the stirred mixture was heated at 80° C for 16 h. After cooling to room temperature, the H_2 was released, and the black reaction mixture discharged. The clear supernatant solution was separated from the iron pigment, and the iron was washed with 1.5 l of THF. The residue was stirred with 1.5 l of THF and 0.4 l of ethanol until the gas evolution had ceased and was then washed again with 1.5 l of THF. After drying under high vacuum (0.1 Pa) 63.7 g of acicular iron pigment was obtained: $Fe^{(0)}$ 81.6%, Fe_{total} 87.87%; $M_S = 193.0$ mT cm^3/g, $M_R = 101.3$ mT cm^3/g, $H_C = 82.2$ kA/m.

Regeneration of the carrier triethylborane

The clear reaction solution separated from the acicular iron pigment, while stirred, was admixed dropwise under a protective gas with distilled water, until gas evolution was no longer observed (about 4 to 5 ml). Then 175.8 g (632.4 mmol) of solid $FeSO_4 \cdot 7H_2O$ was added. After 1 to 2 h of stirring, the bright brown solid was filtered off and subsequently washed with portions of THF. The clear filtrate (1130.5 g), according to the ^{11}B-NMR signal (86.24 ppm) and analytical gas chromatography, contains 7.17% (81.1 g = 827.5 mmol) of pure triethylborane. Thus, 98.1% of the carrier triethylborane, based on the carrier complex employed as the starting material, was recovered.

Preparation of iron nickel alloy from Fe_2NiO_4 and $Na[BEt_3H]$ in toluene

In a 250 ml autoclave equipped with a stirrer, 2.33 g (10 mmol) of Fe_2NiO_4 and 60 ml of toluene was admixed with 75 ml of a 1.61 M $Na[BEt_3H]$ solution (120 mmol) in toluene and heated under H_2 pressure (100 bar) at 130°C for 16 h. After cooling to room temperature, the H_2 was released, and a black reaction mixture discharged. The alloy powder was separated from the supernatant clear solution and washed with 200 ml of THF. Then the mixture was stirred with 100 ml of THF and 100 ml of ethanol was added until the gas evolution has ceased and washed twice with 200 ml aliquots of THF successively. The yield of alloy powder after 2 h of drying under high vacuum (0.1 Pa) was 1.55 g. Metal content: Fe 63.67%; Ni 28.99%. X-ray diffractogram (measured with CoK_α radiation and Fe filter): strongest reflection 2Θ: 52.3°; lattice spacing of planes, *d*: 2.03 Å.

Colloidal transition metals and alloys

The preparation of $[Ti(0) \cdot 0.5THF]_x$ has been published elsewhere [10].

Hydrogenation of Ti sponge using colloidal Ti(0) ***3*** *(cf. Figs. 9 and 10)*

A solution of 367 mg (3.0 mmol = 1 wt.%) $[Ti(O) \cdot 0.5THF]_x$ in 150 ml of THF was added to 13.48 g Ti sponge and introduced into an autoclave. H_2 was introduced to a pressure of 100 bar and the reserve cylinder was filled to 150 bar H_2. Within the first 3 h a minimal uptake of H_2 was observed (latent period). After 21 h the H_2 uptake was completed and the H_2 in the autoclave was slowly released. The reaction mixture was discharged under protective gas. The black solution above the TiH_2 powder was siphoned off and the powder was dried for 16 h in vacuum (oil pump). The powder was identified as TiH_2 by X-ray diffraction by comparison with an authentic sample.

Elemental analysis: calc.: H 4.0%; found H 4.0%; particle size, screening analysis: 10.53 g (78%) < 0.2 mm, 2.84 g (21%) > 0.2 mm; SEM: 3.40 μm.

Protonolysis with 5 M HCl: A solution of 0.133 g of TiH_2 (powder < 0.2

mm) was stirred and heated with 20 ml of 5 M HCl saturated with H_2 until dissolution was complete. The evolved H_2 was collected in a gas burette. Determination 1: 146 N ml (97%); Determination 2: 0.127 g, 141 N ml (99%).

*Hydrogenation of Zr sponge using colloidal Ti(0) **3** (cf. Figs. 10 and 11)*

A solution of 464 mg (3.3=mmol 1 wt.%) Ti(O)·0.5THF_x in 150 ml of THF was added to 30.09 g (330 mmol) Zr sponge and introduced into an autoclave which was thermostated under stirring to 90°C. After adding H_2 to a pressure of 100 bar, the hydrogenation process started spontaneously and stopped after several minutes. After 40 h at 90°C and 100 bar H_2 pressure, the autoclave was cooled down and slowly released. The reaction mixture was discharged under protective gas. The black solution above the ZrH_2 powder was siphoned off and the powder dried under vacuum (oil pump) over 16 h. Elemental analysis: calc.: H 1.9%, found: H 1.7%; particle size, screening analysis: 4.02 g (13%) < 0.2 mm, 25.82 g (86%) > 0.2 mm; SEM: 2–20 μm.

*Hydrogenation of a hydride battery alloy using colloidal Ti(0) **3***

A 5.63 g quantity of a hydride battery alloy (Ni 38.2%, Zr 24.3%, Ti 12.8%, V 18.7%, Cr 6.0%, H_2 0.1%) was treated with a solution of 140 mg $[Ti(O)\cdot 0.5\,THF]_x$ (Ti 40.6%) in 50 ml of THF. The solution was removed under reduced pressure and the doped alloy dried in vacuum over 2 h. The evacuated flask containing the alloy was then connected to a gas burette filled with H_2. After filling the flask with H_2, hydrogenation started spontaneously as indicated by a jump in the sample temperature. The H_2 uptake was monitored with a gas burette over 16 h. The hydrogenated alloy contained 0.7 wt.% of H_2.

NR_4^+ protected colloidal metals and alloys via reducing with tetraalkylammonium hydrotriorganoborates: preparation of iridium colloid (cf. Figs. 13 and 14)

A solution of $N(C_8H_{17})_4[BEt_3H]$ in THF (50 ml, 0.37 M) was added within 1 h at room temperature to a stirred suspension of anhydrous $IrCl_3$ (1.84 g, 6.16 mmol) in 200 ml of THF. Almost complete dissolution of the $IrCl_3$ occurred after 16 h at 60°C. After filtration the clear, dark black–brown solution was concentrated in vacuo, and the black–brown, waxy residue was dried for 3 h at room temperature and 0.1 Pa. The product (7.38 g) was soluble in THF, ether, toluene and acetone, but insoluble in ethanol, and contained 10.85% Ir. The residue was suspended in 200 ml technical quality ethanol without protective gas and addition of 20 ml technical quality ether caused a grey–black precipitate to form. It was left to stand for 1 h, before removing the clear supernatant solution by inert gas pressure (Argon) on the liquid surface. The precipitate was washed once with a mixture of 40 ml ethanol/4 ml ether. Drying in vacuum (0.1 Pa, 1 h, room temperature) yielded a grey iridium colloid powder (0.36 g), which was very soluble in THF, soluble in acetone and insoluble in ether, ethanol and toluene. Elemental analysis: Ir 65.55%, N 0.27%, C 19.97%, H 3.49%; mean particle size: 1.5 nm.

NR_4^+ stabilized metal colloids using conventional reducing agents: preparation of palladium colloid

A 0.5 g (2.23 mmol) quantity of $Pd(ac)_2$ and 1 g (1.30 mmol) $N(dodecyl)_4Br$ were dissolved in 110 ml of THF. The flask was evacuated several times and then H_2 was introduced via a gas burette under normal pressure. After a while the solution turns black and after 16 h 60.4 N ml (120%) of H_2 had been taken up. THF was added to give a total volume of 110 ml and on addition of 55 ml of H_2O/Ar, a brown-black precipitate resulted. After standing for 16 h the supernatant liquid was siphoned off and the solid was dried for 3 h in vacuum. The black powder isolated in this manner was redispersible in THF. Yield: 0.27 g (87%); elemental analysis: Pd 76.73%, C 13.19%, H 2.47%, N 1.64%, Br 3.06%; XPS: Pd(0); mean particle size: 1.8 nm.

Preparation of nanoscale platinum powder via platinum colloid (cf. Figs. 16 and 17)

The preparation of the platinum colloid was carried out in an analogous manner to the iridium colloid. Batch: 8.9 g (33.6 mmol) $PtCl_2$; 200 ml 0.336 M $N(C_8H_{17})_4[BEt_3H]$ in THF (67.2 mmol); 1000 ml THF.

In order to isolate the colloid, the waxy residue was dissolved in 2000 ml of technical quality ether without a protective gas. Addition of 200 ml of pure ethanol brings about the formation of a grey-brown precipitate. After letting the solution stand for 1 h, the clear supernatant solution was removed by siphoning off the liquid. The grey-brown precipitate (soluble platinum colloid) thus obtained was washed 4–5 times under inert gas with approx. 200 ml of pure ethanol until the solution is colourless and the colour of the precipitation changed to grey-black. Washing with 200 ml of THF and drying in vacuum yielded a grey-black platinum powder (4.6 g) which was insoluble in common solvents. Metal content: Pt 92.9%; mean particle size: 2.8 nm.

Determination of the initial hydrogenation activity of palladium/C (5% Pd, cinnamic acid test) using the apparatus described in Fig. 18

A 0.2226 g quantity of the palladium catalyst (Table 15, No. 2) was weighed into a 100 ml dropping funnel, the dropping funnel was placed onto the reactor and the complete apparatus was evacuated several times and refilled with H_2. The catalyst in the dropping funnel was subsequently suspended in 20 ml ethanol (DAB 7, equilibrated at 25°C) and transferred into the reactor. 80 ml of a solution of 125 g cinnamic acid per litre ethanol (also equilibrated at 25°C) were then pipetted into the funnel and dropped into the reactor. Afterwards the funnel was rinsed with 20 ml ethanol. The catalyst suspension was equilibrated at 25°C (± 0.2°C). While the reactor was being charged, it was constantly being flushed with H_2. The self-aspirating hollow stirrer was not yet in use. After the pressure equilibrated, the line to the 1 l precision gas burette (mercury-sealed, coupled to a recorder) was opened and the catalyst suspension stirred with a speed of 2000 rpm. The H_2 consumption was registered over a period of 6 min, whereby the first minute was not utilized in the evaluation. Between the second and sixth minute, a H_2 consumption of 441.6 ml was measured. Conversion to normal conditions gives a consumption of 81.2 N ml/min. From this, after considering a 10% content of solvent in the catalyst, an activity of 406 N ml/(g min) can be calculated.

Determination of the initial hydrogenation activity of platinum/C (5% Pt, crotonic acid test) using the apparatus described in Fig. 18

The procedure was performed analogous to that for palladium catalysts except that the substrates used were a suspension of 0.1597 g platinum catalyst (Table 16, No. 3) in 20 ml ethanol and 80 ml of ethanolic crotonic acid solution (72.6 g crotonic acid/l). The H_2 consumption amounted to 324.2 ml which corresponds to 59.6 N ml/min. The activity of the catalyst after taking into account a solvent content of 10% proved to be 415 N ml/(g min).

Determination of the initial hydrogenation activity of rhodium/C (5% Rh, butyronitrile test) using the apparatus described in Fig. 18

A 0.1904 g quantity of the rhodium catalyst (Table 17, No. 8) was weighed into a 100 ml dropping funnel under inert conditions, the dropping funnel connected to the reactor and the complete apparatus was evacuated and refilled with H_2 several times. The catalyst (in the dropping funnel) was subsequently suspended in 50 ml ethanol (air-free, DAB 7) and introduced into the reactor. The dropping funnel was rinsed with an additional 50 ml of ethanol. The reactor was continuously flushed with H_2. The catalyst suspension was treated in presence of H_2 for 5 min, equilibrated at 40°C (±0.2°C), and the stirring speed adjusted to 2000 rpm. After the pressure equilibrated the connection to the mercury-sealed precision gas burette (200 ml) was opened. 10 ml butyronitrile (distilled under Ar) was injected through the septum into the catalyst suspension. The H_2 consumption was registered per minute. The conversion to N ml H_2 per min yields 34.3 N ml/min. Taking into consideration that catalyst contains ca. 10% solvent, the true quantity of catalyst utilized was 0.1714 g, from which a catalyst activity of 263 N ml/(g min) can be calculated.

Determination of the hydrogenation activity of dissolved palladium colloids (cyclohexene test) using the apparatus described in Fig. 18

The procedure was performed analogously to that for the rhodium catalyst except that the substrates used were a solution of a palladium colloid (approx. 5 mg) in 100 ml THF and 10 ml of cyclohexene. The catalyst solution was equilibrated at 25°C without further H_2 pretreatment.

Acknowledgements

The authors gratefully acknowledge the valuable support of the following scientists, companies and institutions: Dr. G. Block and E. Schauf, Krupp Forschungsinstitut GmbH, D-4300 Essen (Germany), for the measurement and interpretation of the X-ray difractograms and scanning electron microscope studies; Dr. M. Ohlinger, BASF AG, D-6700 Ludwigshafen (Germany), for the TEM images reproduced in Fig. 6 and 7 and the magnetic measurements quoted in Table 7; Prof. Dr. W. Keune and Dipl.-Ing. U. von Hörsten, Laboratorium für Angewandte Physik, Universität-Gesamthochschule D-4100 Duisburg (Germany), for the measurement and interpretation of the Mössbauer spectrum shown in Fig 5; Prof. Dr. R. Courths and Dipl.-Phys. B. Heise, Universität-Gesamthochschule D-4100 Duisburg (Germany), for the XPS spectra obtained using an ESCALAB Mark II; Dr. B. Tesche, Fritz-Haber-Institut der Max-Planck-Gesellschaft, D-1000 Berlin (Germany), for numerous TEM images including Fig. 16, 17, and 19, taken with a Siemens Elmiskop 102 and DEEKO 100 at 100 kV and many helpful discussions; Mr. T. Kamino, Hitachi Instruments Engineering Co. Ltd. , 882 Ichige, Katsuta-shi (Japan), for the HRTEM image in Fig. 14 performed with a Hitachi HF 2000 at 200 kV; Dr. Max Otten, Philips Electron Optics, Eindhoven (The Netherlands), for the HRTEM image shown in Fig. 15 including the EDX point analysis performed at a Philips CM 20 FEG at 200 kV. The result shown in Fig. 9 was obtained with the help of Dipl.-Ing. B. Spliethoff, MPI für Kohlenforschung. Further we are indebted to Drs. R. Brand and A. Freund, Degussa AG, ZN Wolfgang, D-6450 Hanau (Germany), for a gift of commercial noble metal catalysts and the corresponding test procedures. The English of the manuscript was revised by Dr. W. V. Dahlhoff, MPI für Kohlenforschung, to whom the authors express their sincere thanks.

References

1 (a) R. Kieffer and F. Benesovsky, Ullmanns Encykl. Tech. Chem. 4. Aufl., 19 (1980) 563; (b) K.H. Roll, Kirk-Othmer, Encycl. Chem. Tech. 3. Aufl., 19 (1982) 28.
2 R. Krabetz and W.D. Mross, Ullmanns Encykl. Techn. Chem. 4. Aufl., Vol. 13, 517.
3 S.C. Davies and K.J. Klabunde, Chem. Rev., 82 (1982) 152.
4 N. Ibl, Chem. Ing.-Tech., 36 (1964) 601.
5 R.D. Rieke, Organometallics, 2 (1983) 377.
6 H. Bönnemann, B. Bogdanovic, R. Brinkmann, D.-W. He and B. Spliethoff, Angew. Chem. Int. Ed. Engl., 22 (1983) 728.
7 H. Bönnemann, B. Bogdanovic, R. Brinkmann, D.-W. He and B. Spliethoff, J. Organomet. Chem., 451 (1993) 23.
8 H. Bönnemann, W. Brijoux and Th. Joussen, Angew. Chem. Int. Ed. Engl., 29 (1990) 273.
9 USP 5,053,075 (Oct. 1, 1991) to H. Bönnemann, W. Brijoux and R. Brinkmann, Studiengesellschaft Kohle mbH.

10 H. Bönnemann and B. Korall, Angew. Chem., 104 (1992) 1506, Angew. Chem. Int. Ed. Engl., 31 (1992) 1490.

11 H. Bönnemann, W. Brijoux, R. Brinkmann, E. Dinjus, Th. Joussen and B. Korall, Angew. Chem. Int. Ed. Engl., 30 (1991) 1312.

12 H. Bönnemann, R. Brinkmann, R. Köppler, P. Neiteler and J. Richter, Adv. Mater., 4 (1992) 804.

13 (a) H.I. Schlesinger, H.C. Brown, A.E. Finholt, J.R. Gilbreath, H.R. Hoekstra and E.K. Hyde, J. Am. Chem. Soc., 75 (1953) 215; (b) H.C. Brown and C.A. Brown, J. Am. Chem. Soc., 84 (1962) 1492.

14 A. Corrias, G. Ennas, G. Licheri, G. Marongin and G. Paschina, Chem. Mater., 2 (1990) 363.

15 N.N. Greenwood and A. Earnshaw, Chemistry of the Elements, Pergamon, Oxford, 1986, p.189.

16 (a) P. Binger, G. Benedikt, W. Rotermund and R. Köster, Liebigs Ann. Chem., 717 (1968) 21; (b) R. Köster, Methoden Org. Chem. (Houben-Weyl) 4. Aufl., 13b (1983) 798.

17 (a) DE OS 3934351 (18.04.91), to H. Bönnemann, W. Brijoux and Th. Joussen, Studiengesellschaft Kohle mbH; (b) EP OS 0423627 (24.04.91), to H. Bönnemann, W. Brijoux and Th. Joussen, Studiengesellschaft Kohle mbH.

18 R.G. Pearson, Surv. Prog. Chem., 5 (1969) 1.

19 L. Kolditz (Ed.), Anorganikum, Teil 1, VEB Deutscher Verlag der Wissenschaften, Berlin, 1981, 474 pp.

20 J.D'Ans and E. Lax, Taschenbuch für Chemiker und Physiker, 3rd Ed., 1 (1967) 1.

21 H.P. Klug and L.E. Alexander, X-Ray Diffraction Procedures for Polycrystalline and Amorphous Materials, 2nd Edit., Wiley, New York, 1974.

22 (a) J. van Wonterghem, S. Mørup, C.J.W. Koch, S.W. Charles and S. Wells, Nature, 322 (1986) 622; (b) J. van Wonterghem and S. Mørup, Hyperfine Interact. 42 (1988) 959.

23 C.E. Johnson, M.S. Ridout and T.E. Cranshaw, Proc. Phys. Soc., (1963) 1079.

24 D. Zeng and M.J. Hampden-Smith, Chem. Mater. 4 (1992) 968.

25 USP 5,053,075 (Oct. 1, 1991) to H. Bönnemann, W. Brijoux and R. Brinkmann, Studiengesellschaft Kohle mbH.

26 (a) EP 0015 485 (26.02.1980) to G. Schroeder, G. Buxbaum, F. Hund, H. -C. Schopper and R. Naumann, Bayer AG; (b) USP 2,900,246 (Sept. 14, 1965) to H.C. Miller and A.L. Oppegard, E.I. du Pont.

27 (a) J.S. Bradley, Adv. Organomet. Chem., 22 (1983) 1; (b) J.S. Bradley, E. Hill, M.E. Leonowicz and H.J. Witzke, J. Mol. Catal., 41 (1987) 59; (c) J.S. Bradley, J.M. Millar, E.W. Hill, S. Behal, B. Chaudret and A. Duteil, Faraday Discuss, 92 (1991) 225.

28 (a) K. Esumi, M. Shiratori, H. Ishizuka, T. Tano, K. Torigoe and K. Meguro, Langmuir, 7 (1991) 457; (b) K. Meguro, M. Torizuka and K. Esumi, Bull. Chem. Soc. Jpn., 61 (1988) 341; (c) K. Esumi, M. Suzuki, T. Tano, K. Torigoe and K. Meguro, Colloids Surf., 55 (1991) 9; (d) T. Tano, K. Esumi and K. Meguro, J. Colloid Interface Sci., 133 (1989) 530.

29 (a) K.J. Klabunde, Y.-X. Li and B.J. Tan, Chem. Mater., 3 (1991) 30; (b) K.J. Klabunde, Science, 224 (1984) 1329; (c) K.J. Klabunde and Y. Imizu, J. Am. Chem. Soc., 106 (1984) 2721; (d) K.J. Klabunde and Y. Tanaka, J. Mol. Catal., 47 (1982) 843.

30 (a) L.N. Lewis and N. Lewis, Chem. Mater., 1 (1989) 106; (b) L.N. Lewis and L.N. Lewis, J. Am. Chem. Soc., 108 (1986) 7228; (c) L.N. Lewis, R. Uriarte and N. Lewis, J. Catal., 127 (1991) 67.

31 (a) T.A. Stromnova, I.N. Busygina, M.N. Vargaftik and I.I. Moiseev, Metalloorg. Khim., 3 (1990) 803; (b) I.I. Moiseev, Pure Appl. Chem., 61 (1989) 1755; (c) I.I. Moiseev, Mekh. Katal. Novosibirsk, (1984) 21 (Ref. Zh., Khim. (1985), Abstr. No. 4B4121); (d) I.I. Moiseev, Itogi Nauki Tekh. VINITI Kinet. Katal. (1984) 13 (Ref. Zh., Khim. (1984), Abstr. No. 16B4121).

32 (a) G. Schmid, Endeavour, 14 (1990) 172; (b) G. Schmid, Aspects Homogen. Catal., 7 (1990) 1; (c) G. Schmid, H.H.A. Smit, M.P.J. Staveren and R.C. Thiel, New J. Chem., 14 (1990) 559; (d) G. Schmid, N. Klein, B. Morun, A. Lehnert and J.O. Malm, Pure Appl. Chem., 62

(1990) 1175; (e) L.J. De Jongh, J.A.O. De Aguiar, H.B. Brom, G. Longoni, J.M. Van Ruitenbeek, G. Schmid, H.H.A. Smit, M.P.J. Van Staveren and R.C. Thiel, Z. Phys. D: At., Mol. Clusters, 12 (1989) 455.

33 (a) N. Toshima, M. Harada, T. Yonezawa, K. Kushihashi and K. Asakura, J. Phys. Chem., 95 (1991) 7448; (b) N. Toshima and T. Takahashi, Bull. Chem. Soc. Jpn., 65 (1992) 400; (c) N. Toshima, T. Takahashi and H. Hirai, J. Makromol. Sci., Chem., A25 (1988) 669; (d) N. Toshima, J. Macromol. Sci., Chem., A27 (1990) 1225; (e) Zhao Bin and N. Toshima, Chem. Express, 5, No. 10 (1990) 721.

34 H. Bönnemann, W. Brijoux, R. Brinkmann, E. Dinjus, R. Fretzen, Th. Joussen, B. Korall, J. Mol. Catal., 74 (1992) 323.

35 B. Bogdanovic, T. Hartwig, A. Ritter, K. Strassburger and B. Spliethoff, Abschlussbericht zum BMFT-Forschungsvorhaben Nr. 0328939 C (1991).

36 (a) J. Blum, Y. Sasson and A. Zoran, J. Mol. Catal., 11 (1981) 293; (b) J.Blum, I. Amer, K.P.C. Vollhardt, H. Schwarz and G. Höhne, J. Org. Chem., 52 (1987) 2804; (c) I. Amer, V. Orshaw and J. Blum, J. Mol. Catal., 45 (1988) 207; (d) I. Amer, T. Bernstein, M. Eisen, J. Blum and K.P.C. Vollhardt, J. Mol. Catal., 60 (1990) 313; (e) I. Amer, J. Blum and K.P.C. Vollhardt, J. Mol. Catal., 60 (1990) 323; (f) Y. Badrieh, J. Blum, I. Amer and K.P.C. Vollhardt, J. Mol. Catal., 66 (1991) 295; (g) J. Blum, H. Huminer and H. Alper, J. Mol. Catal., 75 (1992) 153; (h) Y. Badrieh, A. Kayyal and J. Blum, J. Mol. Catal., 75 (1992) 161; (i) DOS 3 841 698 (1989) to A. Laufenberg, A. Behr and W. Keim, Henkel KGaA; (j) N. Satoh, K. Kimura, Bull. Chem. Soc. Jpn., 62 (1988) 1758.

37 R. Willstätter and E. Waldschmidt-Leitz, Ber. Dtsch. Chem. Ges., 54 (1921) 113.

38 L.L. Hegedus (Ed.), Catalyst Design, Wiley, New York, 1987.

39 S.A. Stevenson (Ed.), Metal-Support Interactions in Catalysis, Sintering and Redispersion, Van Nostrand Reinhold, New York, 1987.

40 (a) O.S. Alekseev, V.I. Zaikovskii and Y.A. Ryndin, J. Appl. Catal., 63 (1990) 37; (b) Y.A. Ryndin, O.S. Alekseev, P.A. Simonov and V.A. Likholobov, J. Mol. Catal., 55 (1989) 109; (c) Y.A. Ryndin, O.S. Alekseev, E.A. Paukshtis, A.V. Kalinkin and D.I. Kochubey, Appl. Catal., 63 (1990) 51.

41 DE WO/92/18246 (07.04.92) to H. Bönnemann, W. Brijoux, R. Brinkmann, E. Dinjus, R. Fretzen and B. Korall, Studiengesellschaft Kohle mbH.